Cable Stay Fatigue Analysis for the Fred Hartman Bridge

by

John C. Eggers, B.S.C.E.

Thesis

Presented to the Faculty of the Graduate School of

The University of Texas at Austin

in Partial Fulfillment

of the Requirements

for the Degree of

Master of Science in Engineering

The University of Texas at Austin

August 2003

Cable Stay Fatigue Analysis for the

Fred Hartman Bridge

Approved by
Supervising Committee:

Dr. Sharon Wood, Supervisor

Dr. Karl Frank, Supervisor

Dedication

I would like to dedicate this thesis to my parents, my father and mother in-law, and my beautiful, patient, and loving wife, Jennifer.

Acknowledgements

I would like to thank the Texas Department of Transportation for sponsoring this project at the Ferguson Structural Engineering Laboratory (FSEL) at The University of Texas at Austin.

I would like to also give my appreciation to the many professors that assisted in my research. Specifically I would like to thank Dr. Sharon Wood and Dr. Karl Frank for their advice and dedication to this project.

A large amount of manual labor was required for this project. I would like to thank Tammer Botros and Meg Warpinski for their companionship, labor, and ideas throughout the project. The lab technicians who include Blake Stassney, Mike Bell, and Dennis Fillip provided invaluable assistance throughout the project. Their experience and knowledge of the laboratory environment provide an enormous amount of assistance to every research project at FSEL.

I would also like to thank my fellow graduate students for making life at FSEL and The University of Texas enjoyable.

May 2003

Abstract

Cable Stay Fatigue Analysis for the

Fred Hartman Bridge

John C. Eggers, M.S.E.

The University of Texas at Austin, 2003

Supervisors: Sharon Wood, Karl Frank

Topics covered in this thesis include analysis and testing of single-strand specimens under tension and static bending loads, including the development of closed-form solutions to estimate the bending moment in a single strand under tension and bending. It also includes tensile fatigue characterization of strand. In addition, there is the characterization and analysis of vibration data from the Fred Hartman Bridge, including integration of acceleration data to attain displacement records and rainflow cycle counting analyses.

Table of Contents

List of Tables

List of Figures

CHAPTER 1
Introduction

1.1 FRED HARTMAN BRIDGE

Construction was completed on the Fred Hartman Bridge (Fig. 1.1) on September 27, 1995. The bridge crosses the Houston shipping channel between Baytown and La Port, Texas and was constructed to replace the Baytown-La Porte Tunnel.

Figure 1.1 Fred Hartman Bridge

One of the most remarkable aspects of the Fred Hartman Bridge is its extreme width of 160 ft (49 m). The bridge is composed of two independent decks, each 78 ft (24 m) wide (Fig. 1.2). Each deck accommodates four lanes of traffic and two emergency lanes. In terms of overall deck area, the Fred Hartman Bridge is one of the largest cable-stayed bridges in the world.

Figure 1.2 Two Independent Deck of the Fred Hartman Bridge

The following is a summary of information about the Fred Hartman Bridge (National Web Window, 2001):

- Total length: 2,475 ft
- Main span: 1250 ft
- Building time: 9 years from 1986 until 1995
- Capacity: 200,000 vehicles per day (Baytown tunnel: 25,000 per day)
- Cost: 100 million US Dollars
- Double diamond towers - 436 ft (133 m) tall
- Fan-type arrangement of the stay cables
- 192 cables, the longest stretching 650 ft (198 m)
- Over 618 miles of cable strand
- More than 40,000,000 pounds (18,145 t) of steel
- More than 3,000,000 ft^3 (48,951 m^3) of concrete

1.2 CABLE VIBRATION PROBLEMS

Since construction, wind-rain induced vibrations have been observed in the stay-cables of the Fred Hartman Bridge. Wind-rain induced vibrations are produced when rainwater forms rivulets under the influence of the airflow around the cable, which then changes the aerodynamic cross section of the stay cable in such a way that it is susceptible to vibrations (Poser 2002). The Texas Department of Transportation (TXDoT) has since initiated a research project to:

- Design repair solutions for existing damage caused by the vibrations

- Design structural and aerodynamic solutions to eliminate or control cable vibrations
- Characterize the vibrations so the mechanics are better understood and efficient damping can be designed to control the vibrations
- Characterize the fatigue behavior of the cables and estimate the amount of fatigue damage caused by the wind-rain induced vibrations

Engineers from Whitlock, Dalrymple, Poston, and Associates (WDP), Johns Hopkins University (JHU), Texas Tech University (TTU), and the University of Texas at Austin (UT) form the team developed by TxDOT to investigate the wind-rain induced vibration phenomenon observed on the Fred Hartman Bridge.

WDP developed designs to repair the existing damage, and reduce the cable vibrations. Solutions that have been installed include the following:

- stiffened guide pipe connections to withstand the large forces induced by cable vibrations
- installation of cable restrainers which allow cables that are excited by wind-rain induced vibration to be restrained by adjacent cables to reduce the effective length of the cables
- installation of dampers which reduce the amplitude of the vibrations

Researchers from Johns Hopkins University instrumented several cables on the Fred Hartman Bridge in October of 1997 to identify the vibrational characteristics. The vibrational characteristics are essential for understanding the mechanics of the wind-rain vibrations and to design efficient damping solutions. Researchers from JHU have developed a statistical database containing cable

vibration characteristics and weather data for each recorded vibration event since October 1997.

Researchers from Texas Tech University developed an aerodynamic damping solution. Their proposed solution consists of a number of rings wrapped around the cable to prevent the formation of the rainwater rivulets (Sarker 1999).

The research team from the University of Texas (UT) has focused on characterizing the fatigue behavior of the cables. The research program consists of three phases:

1. Instrument the stay cables on the Fred Hartman Bridge to determine the relationship between measured strains and accelerations during a wind-rain vibration event
2. Assemble and test ten full-size fatigue tests in the laboratory to determine their fatigue behavior
3. Develop computational models of the full-sized test specimens and the Fred Hartman stay cables. Use the models to relate the observed fatigue behavior of the test specimens to cables with different lengths and diameters on the bridge.

1.3 RESEARCH CONDUCTED AT THE UNIVERSITY OF TEXAS

1.3.1 Field Measurments

As of May 2003, the research team at UT has attempted to measure strains at various locations on the Fred Hartman Bridge. The exterior polyethylene (PE) sheathing of the stay cables, the surface of the grout just below the PE sheathing, and the guide pipes attaching the cables to the deck. The field measurements were largely unsuccessful. For various reasons, the strain gages either did not

adhere correctly, corroded rapidly, or provided limited data (Poser 2001). Future attempts to gage the cables are not planned.

The accelerations of the stay cables were monitored by the JHU research team. Although the monitoring system was not completely reliable, these accelerometers have provided useful data during wind-rain induced vibrations. It is anticipated that researchers at the University of Texas will be able to correlate these data to stress with using the computational models.

1.3.2 Full-Scale Bending Fatigue Testing

As of May 2003, five full-size cable stay fatigue tests have been completed. Each test specimen was constructed similar to the smallest stay cable on the bridge, and the length of each specimen was approximately 33 ft. For each test, parameters such as the grout mix design, transverse displacement amplitude, and other construction variables were varied. An overview of the 5 full-sized tests is shown in Table 1.1. The 2001 thesis by Poser documents the behavior of the first two specimens.

Table 1.1Full-Sized Specimen Test Summary

Specimen No.	Displacement Amplitude (+/- in.)	Testing Frequency (Hz)	Total Number of Cycles
1	1.60	0.9	2,808,398
2	1.60	0.7	2,865,103
3	1.60	2.2	4,961,560
4	1.10	3.0	8,775,245
5*	1.60	3.0	5,211,056

* Specimen 5 was ungrouted and there were no wire failures

1.3.3 Computational Models

Previously on this project, Dowd (2001) developed a finite element model (FEM) of the full-scale strand specimen using beam elements and transformed sections. Comparison of the FEM model and the results of the full-scale test described above indicated that the FEM model overestimates the cable stiffness by nearly a factor of 2. Further refinement of the FEM model is needed to develop a more realistic model of the test specimens.

1.4 TOPICS COVERED IN THIS THESIS

This thesis describes research activities related to three different components of the UT research project. While this thesis does not discuss the results of the full-scale tests or the development of the computational models specifically, it does describe research related to the research at UT. Topics covered in this thesis include analysis and testing of single-strand specimens under tension and static bending loads, tensile fatigue characterization of strand used to construct full-scale specimens 1 through 6, and characterization and analysis of vibration data from the Fred Hartman Bridge.

1.4.1 Single Strand Bending Tests

Chapter 2 of this thesis describes the testing of three single-strand specimens under tension and static bending and the development of closed-form solutions. The closed-form solutions are intended to bound the stiffness of the single-strand specimens and are used to estimate the moment in the strand. Comparisons are made between the closed-form solutions, single-strand results, and the results of the full-scale specimens.

An estimate of the single-strand stiffness is developed based on the closed-form solution, using an effective moment of inertia and modulus (effective

EI). The results from this phase of the research will be used by the research team to refine the computational models.

1.4.2 Fatigue Tests of Strand in Tension

Tension fatigue tests were used to establish the fatigue characteristics of the strand used to construct the first six, 19-strand stay cable specimens. Chapter 3 describes the testing procedure, presents the results, and compares the results with specified design criteria and other published strand fatigue data. The results of the strand fatigue tests will be used by the research team to characterize the axial fatigue performance of the strand.

1.4.3 Characterization of Cable Vibration Data from the Fred Hartman Bridge

Data from JHU is used to characterize the cable motions in Chapter 4 of this thesis. Acceleration data from wind-rain vibration events are used to calculate the displacement history during ten different wind-rain events. The displacement histories are used to characterize the vibration of the cables in terms of Lissajous diagrams and mode number.

The displacement histories for each cable are characterized using rainflow counting and the results are used to develop an equivalent displacement for each cable. Next, statistical data compiled by researchers at JHU are used to estimate the amount of time that each of the cables has experienced wind-rain induced vibrations. These results are compared with the observed fatigue life of the first five stay cable specimens.

The results of the vibration characterization are in the form of an equivalent displacement at the location of the accelerometer and an estimated number of cycles that the cable has experienced since construction. After refinement of the computational model, the research team should be able to use

the results of the cable fatigue characterization and the cable stay tests to estimate fatigue damage and the remaining life of the stay cables that support the Fred Hartman Bridge.

CHAPTER 2

Single-strand Bending Tests

This chapter explains the development of simplified closed-form solutions for single-strand bending and describes the testing of single 0.6-in., 7-wire strand under tension and bending.

2.1 INTRODUCTION

Analysis of stay cables under tension and bending loads is a complex problem. The interactions between the grout and strands and the relative movement of the wires within each strand are not fully understood. Previously on this project, analysis and testing of full-scale cable specimens was performed (Dowd 2001, Poser 2001). The full-scale specimens were 19-strand cables, 33 feet in length and similar in design to cables constructed on the Fred Hartman Bridge. Each was pre-stressed to 40 percent of the guaranteed ultimate strength and bending was induced by imposing a mid-span deflection.

Dowd (2001) developed a finite element model of the full-scale strand specimen using beam elements and transformed sections. Table 2.1 shows a comparison of the transverse load calculated using that FEM model for a mid-span deflection of 1.6 in. (Dowd 2001) and the measured transverse load for specimens one and two for a mid-span deflection of 1.6 in. (Poser 2001).

Table 2.1 Difference between FEM and Measured Response

	FEM	Measured*	Difference
Prestress Force (kip):	445	445	-
Mid-span Deflection (+/- in.):	1.6	1.6	-
Transverse Force (+/- kip):	16.0	7.6	8.4

*Measured values are identical for both specimen 1 and specimen 2

As shown in Table 2.1, the transverse load estimate from the FEM analysis overestimates the measured transverse load by more than a factor of 2. Further refinement of the FEM model is needed to develop a more realistic model of the test specimens. In order to understand the response of the cable, attempts were made to measure the strain in the strand at various locations in the grouted specimen. Unfortunately, it was difficult to obtain useful strain data. Grouting and stressing the strand damaged the strain gages attached to the strand and the research team was unable to find an appropriate adhesive for attaching the strain gages to the polyethylene pipe.

Because of the difficulties encountered in measuring the strain response of the grouted, 19-strand specimens, tests of an ungrouted, single-strand specimen were planned. The results of these tests should assist the development of a refined FEM model for the grouted 19-strand specimen. For comparison, closed-form solutions were also developed for a single strand under tension and bending.

2.2 CLOSED-FORM SOLUTIONS

Two closed-form solutions were developed for a single strand subjected to tension and bending due to lateral loading. In the first solution, a simply-supported beam with axial tension was subjected to a transverse load at mid-span. In the second, the ends of the beam were assumed to be fixed against rotation.

The two solutions represent lower and upper bounds for the stiffness of a single strand.

The simply-supported solution is meant to be the lower bound for the stiffness because the strand has some rotational restraint at the ends due to the face of the chucks bearing on the test frame. Note that the simply-supported solution has no reaction moment.

The fixed end beam solution is meant to be the upper bound solution for two reasons. First, it is believed that the ends of the strand are only partially restrained against rotation. Second, the EI used in the fixed end beam solution assumes a solid beam cross section but the strand is composed of seven separate wires. These wires can slip relative to each other unlike a solid cross section, resulting in a response that is less stiff than the fixed end solution (Papaoliou, 1999). Note that because the fixed end solution does have reaction moments, the moment diagram near the supports should also be an upper bound solution for the moment in the strand.

The derivation of both closed-form solutions assumes the same basic parameters. First, the strand is viewed as a tension strut with a transverse force at mid-span (Fig. 2.1). Second, to include secondary bending effects due to the tension in the strand, the free-body diagram (FBD) includes an initial deflection due to the transverse load (Fig. 2.2). This is similar to the derivation of a compression member with secondary bending (i.e. Euler buckling), except the solution is stable due to the tension in the strand. Deformation due to shear was ignored due to the large span-to-depth ratio of the strand. Because the transverse load is located at mid-span, the solutions are symmetric. Therefore the solutions are derived for only half of the beam, and $0 \le x \le L/2$.

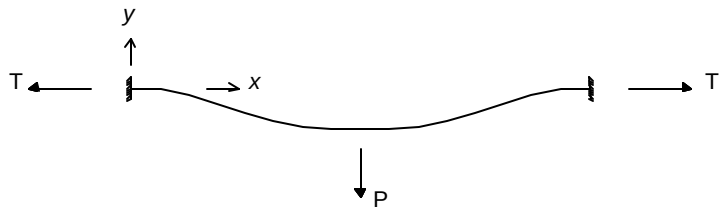

Figure 2.1 Model for Tension Strut with Transverse Load at Mid-Span

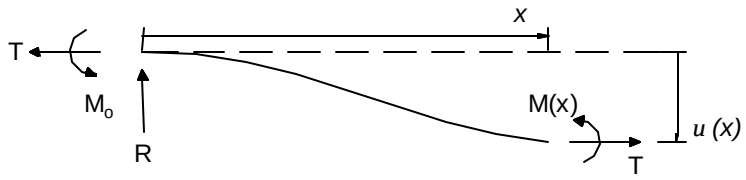

Figure 2.2 Free Body Diagram Including Initial Deformation

Equation 2.1defines the moment equilibrium equation for the deformed strand:

$$M(x) = Rx - Tu(x) - M_0 \qquad (2.1)$$

where R is the reaction at the left support, T is the tensile force, $\upsilon(x)$ is the transverse deflection at location x, and M_0 is the moment at the left support. Equation 2.1 is obtained from the free body diagram (Fig. 2.2) by summing moments about an arbitrary location x. Substituting the relationship between moment and curvature for an elastic member (Eq. 2.2), the vertical reaction at the left end for a symmetric loading condition (Eq. 2.3), and defining the parameter λ^2 (Eq. 2.4), yields the governing differential equation (Eq. 2.5):

$$M(x) = -EI\frac{d^2u(x)}{dx^2} \tag{2.2}$$

$$R = \frac{P}{2} \tag{2.3}$$

$$l^2 = \frac{T}{EI} \tag{2.4}$$

$$\frac{d^2u(x)}{dx^2} - l^2u(x) = \frac{-P}{2EI}x + \frac{M_0}{EI} \tag{2.5}$$

The moment of inertia (I) of the strand is calculated using the actual cross sectional shape and area of the strand, but assuming that the individual wires do not slip relative to each other. The calculated moment of inertia is 4.291×10^{-3} in^4. The modulus of elasticity (E) is assumed to be 28,000 ksi based in the strand manufacturer's specification sheet (Fig. B.16). The tension in the strand (T) is 23.6 kips, which produces the same tensile stress used in the 19-strand specimens and the Fred Hartman Bridge cables. The length (L) of the beam is 33 ft. The complete derivation of each of the closed-form solutions is presented in Appendix A.

2.2.1 Fixed End Beam Subjected to Axial Tension and Bending

The model used for the fixed end beam is shown in Figure 2.4., and the reaction moments are included in this solution. The corresponding variations of transverse deflection, slope, and curvature are given in equations 2.8 through 2.10.

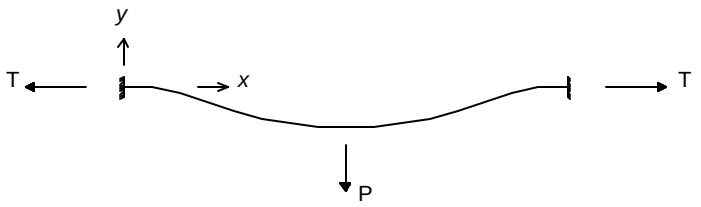

Figure 2.3 Model for Fixed End Beam

$$u(x) = \frac{-P}{2Tl}\sinh(lx) + \frac{M_0}{T}\cosh(lx) + \frac{P}{2T}x - \frac{M_0}{T} \qquad (2.5)$$

$$\frac{d}{dx}u(x) = \frac{-P}{2T}\cosh(lx) + \frac{M_0}{T}\sinh(lx) + \frac{P}{2T} \qquad (2.6)$$

$$\frac{d^2}{dx^2}u(x) = \frac{-P}{2T}\,l\sinh(lx) + \frac{M_0}{T}\cosh(lx) \qquad (2.7)$$

The transverse stiffness corresponding to this model with a tension force of 23.6 kip is 257 lb/in. The maximum moment for the fixed end beam, which occurs at the ends, is 586 lb-in. for a transverse load of 514 lb. Figure 2.5 shows the moment for the first 12 in. of the fixed end solution. Note that the moment is essentially zero at 12 in. from the face of the chuck. The deflected shape and moment diagrams for the fixed end beam solution are plotted for a mid-span deflection of 2.0 in. are in Appendix A.

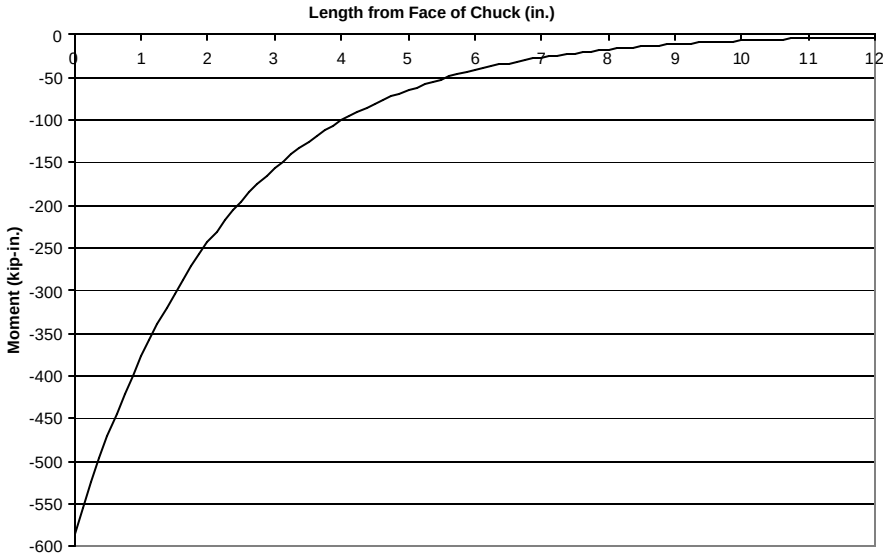

Figure 2.4 Moment Diagram for Fixed end Beam

2.2.2 Simply-Supported Beam Subjected to Axial Tension and Bending

The model used for the simply-supported beam is shown in Figure 2.3, and the reaction moments are zero. The corresponding variations of transverse deflection, slope, and curvature are given in equations 2.5 through 2.7. Although presented in a different form, the results are identical to those given by Timoshenko (1956). Note that equations 2.8 through 2.10 are identical to equations 2.5 through 2.7 with the exception that the end moment, M_0, is equal to zero for the simply-supported beam.

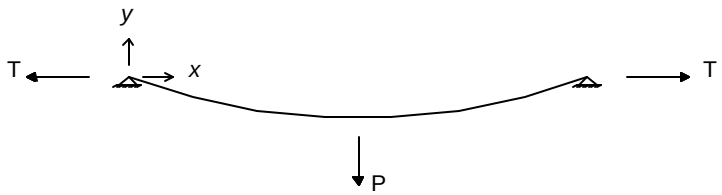

Figure 2.5 Model for Simply-Supported Beam

$$u(x) = \frac{-P}{2Tl}\frac{\sinh(lx)}{\cosh(lL/2)} + \frac{P}{2T}x \tag{2.8}$$

$$\frac{d}{dx}u(x) = \frac{-P}{2T}\frac{\cosh(lx)}{\cosh(lL/2)} + \frac{P}{2T} \tag{2.9}$$

$$\frac{d^2}{dx^2}u(x) = \frac{-Pl}{2T}\frac{\sinh(lx)}{\cosh(lL/2)} \tag{2.10}$$

The transverse stiffness corresponding to a model with a tensile force of 23.6 kip is 241 lb/in., where transverse bending stiffness is defined as P divided by mid-span deflection. The deflected shape and moment diagram for the simply-supported solution are plotted for a mid-span deflection of 2.0 in. are in Appendix A. The simply-supported solution provides a lower bound for the transverse bending stiffness of the single-strand. The maximum moment for the simply-supported beam, which occurs at the mid-point, is 549 lb-in. for a transverse load of 482 lb. Because the end moments are zero, the moment diagram represents the upper bound for the moment at mid-span of the strand.

2.3 SINGLE-STRAND TESTS

Static load tests were performed on single-strands and then compared with the results of the closed-form solutions. The tests were comprised of a single-strand under tension with an applied load at mid-span.

2.3.1 Test Apparatus

The test frames used for the single-strand tests were the same frames used for the full-scale, bending fatigue tests (Poser 2001). Test frames consisting of two longitudinal wide flange columns and built up crossbeams at both ends were used to react the initial stressing force and the forces from the single-strand test. Two longitudinal W14x90 columns serve as axial compression members to provide reaction to the prestress force in the strand (Fig. 2.6). The built up crossbeams at both ends consist of two W18x97 beams with welded stiffeners and a load distribution plate with an opening for the strand. The load distribution plate is in direct contact with the strand chuck and directs the forces from the strand into the test frame (Fig. 2.7). To provide reaction to the vertical shear forces the frame was anchored to the laboratory floor.

For each test, a chain hoist hanging from an overhead arm was attached to the strand and used to impose deformations at mid-span of the strand (Figure 2.6). The magnitude of the tensile load in the strand and the applied transverse load were measured using load cells. The mid-span deflection was measured using a linear potentiometer. In addition, strain gages were attached to individual wires of the strand near the face of the chuck at the dead end of the specimen.

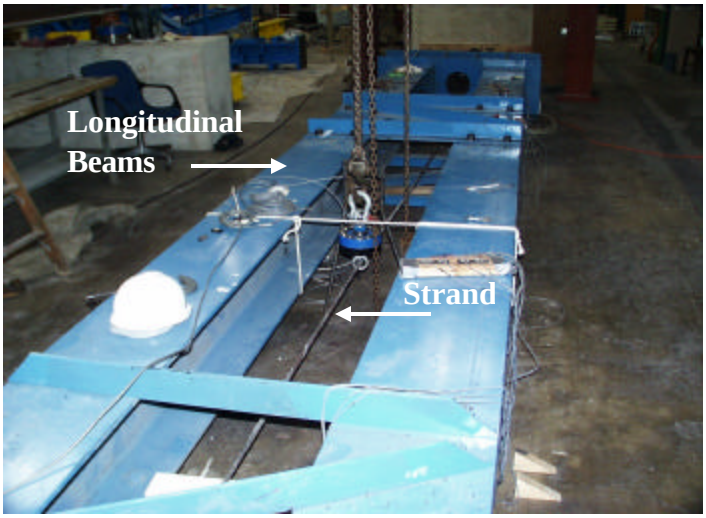

Figure 2.6 Test Frame with Specimen Installed

For each test, a single 0.6 in., 270 ksi, 7-wire strand was placed in the test frame. The strand was then tensioned to approximately 23.6 kips which is 40% of the guaranteed ultimate tensile strength, the same stress used for the full-sized specimens and the Fred Hartman Bridge stay cables. The area of the strand used to calculate the stress was 0.2185 in. and this area was verified by UT researchers (Fig. B.17). Stressing was performed using a single-strand hydraulic ram and held in place with reusable chucks (Fig. 2.7). The total length of each specimen was 33 feet, which was measured from the inside face of chuck to the inside face of chuck. The transverse displacement at mid-span was increased from 0 to 2 in. in increments of approximately 0.1 in. during each test. All loads were applied statically.

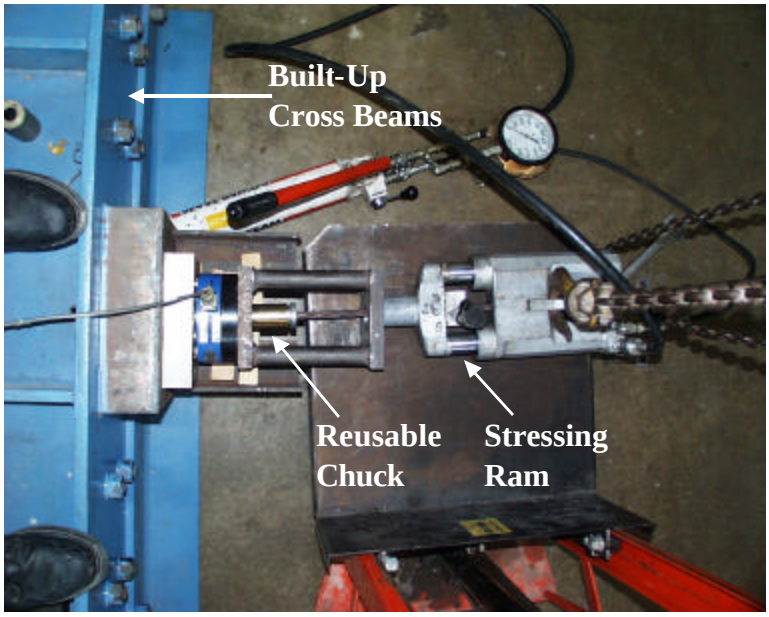

Figure 2.7 Stressing of Single-strand

2.3.2 Measured Response

Three different sections of strand from a single spool were tested: strand 1, 2, and 3. Tests were conducted at different levels of prestress: test 1, 2, and 3. All of the tests were repeated at least twice at the same pre-stress level to duplicate the results. All the results from replicated tests were within 5%. The strand used in the study satisfies ASTM A416 and was manufactured by American Spring Wire (ASW) Corporation in Houston, Texas. The specification sheet from ASW for the specific heat tested is included in Appendix B. The results presented in Sections 2.3.2.1 and 2.3.2.2 summarize important results from all three tests. The complete set of measured data is presented in Appendix B in the form of transverse load-deflection plots.

2.3.2.1 Strand Stiffness

The single-strand tests included static tests at values of axial prestress ranging from 7.5 kips to 30.8 kips. The observed stiffness of the strand increased nearly linearly with prestress force as seen in Figure 2.8. Because of the inaccuracies in the stressing equipment, it was difficult to stress the strand to the desired level so a least-squares approach was used to relate the observed stiffness to the applied prestress force (Fig. 2.8). The resulting least-squares linear approximation is shown in Equation 2.11. The corresponding R^2 value is 0.99. Based on these results, the average stiffness of the strand with an axial tension of 23.6 kip was 251 lb/in.

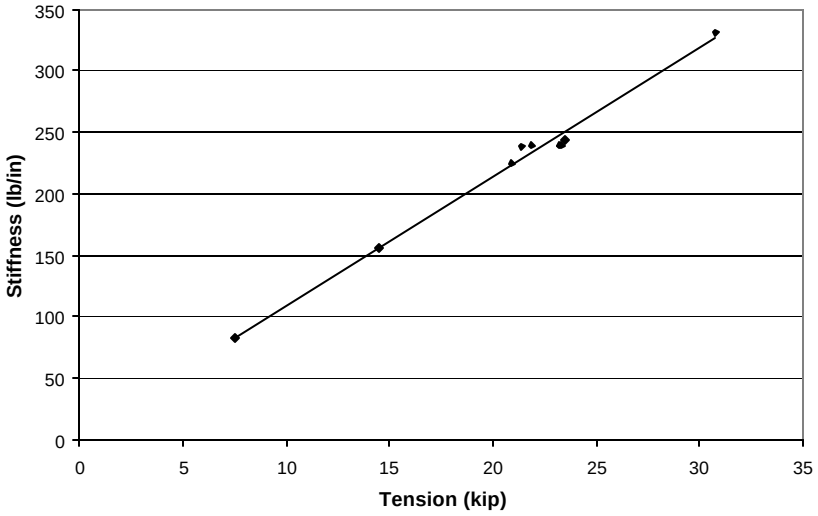

Figure 2.8 Stiffness vs. Prestress Force

$$k = 10.5T + 3.86 = \frac{P}{u_{\max}} \qquad (2.11)$$

Where k is the transverse stiffness of the strand and T is the initial prestress axial force.

The measured stiffness of the single-strand is compared with the measured stiffness of cable stay specimens 1 through 5 in Table 2.2. For comparison the equivalent stiffness per strand is calculated as the measured stiffness of the specimen divided by the number of strands in that specimen. Note that the prestress tension is 108 ksi, 23.6 kip/strand, for all the specimens in Table 2.2. The information about the ungrouted specimen is from cable stay specimen 5, which was constructed and tested in early 2003.

Table 2.2 Measured Stiffness of Various Specimens

	Grouted/Ungrouted	Measured Stiffness (lb/in.)	Number of Strands	Stiffness/Strand (lb/in.)	Difference from Single Strand (%)
Single Strand:	Ungrouted	251	1	251	-
Cable Stay 1*:	Grouted	4750	19	250	-0.4%
Cable Stay 2*:	Grouted	4750	19	250	-0.4%
Cable Stay 3:	Grouted	4685	19	247	-1.8%
Cable Stay 4:	Grouted	4535	19	239	-4.9%
Cable Stay 5:	Ungrouted	4083	19	215	-14.4%

* (Poser 2001)

The effective stiffness per strand is essentially the same for the four grouted specimens and the single-strand in Table 2.2. The full-scale ungrouted specimen (Cable Stay 5) had the largest difference from the single-strand results. The reason for this is unknown and further investigation needs to be performed to identify the cause of this apparent difference.

Note that the measured lateral bending stiffness of the strand was dependent on the amplitude of the lateral deformation. Data are plotted in Figure 2.9 for one loading and unloading cycle. This trend was observed with all the

single-strand tests. The stiffness increases slightly with deflection due to lengthening of the cable and hence increasing its tension (Fig. 2.10). This increase in axial tension due to lengthening was not included in the closed-form solutions. Because the increase in stiffness was approximately 2%, it was considered to be insignificant. The average stiffness is used in all comparisons.

Also, all the tests indicated a reduction in stiffness of between 2% and 5% after the first cycle of deflection (Fig. 2.9). However, the amplitude of the variation decreased after repeated cycles. This may be due to additional seating of the wedges during the first few cycles of each test.

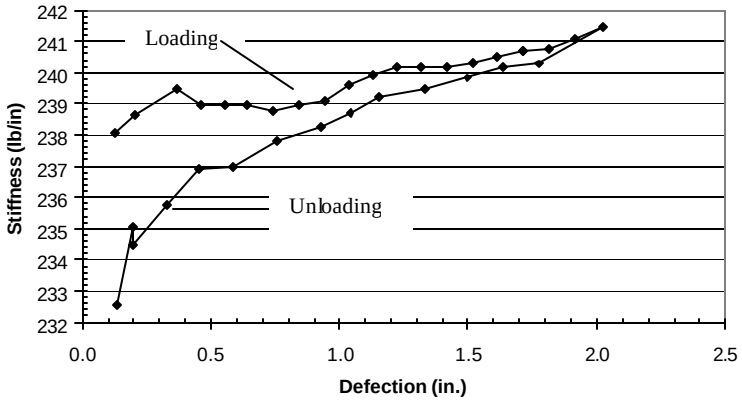

Figure 2.9 Stiffness vs. Deflection of Single-strand for a Prestress Force of 23.3 kip

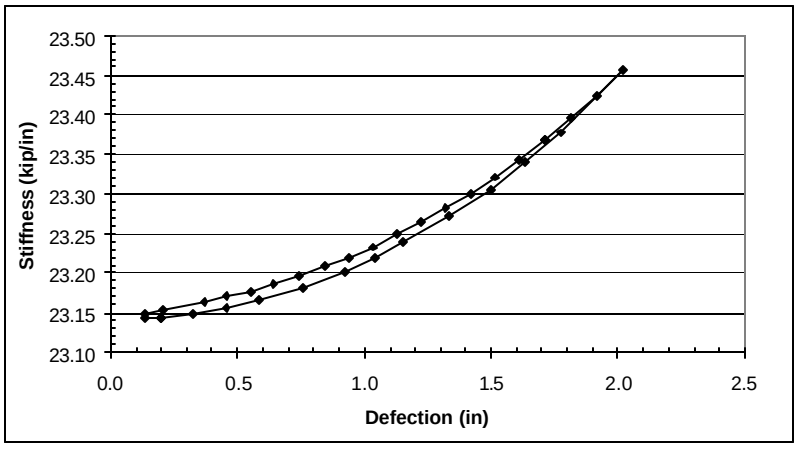

Figure 2.10 Tensile Load vs. Deflection of Single-strand for a Prestress Force of 23.3 kip

2.3.2.2 Strand Strain

Two sets of strain gages were attached to the individual wires of the strand located near the face of the chuck at the dead end of the specimen. The gage location closest to the chuck was labeled location A and the location further from the chuck was labeled location B (Figure 2.11). The distances shown in Figure 2.10 were measured during Test 2 and Test 3 for Strand 3. The actual location of each gage was determined after each test by measuring the distance from the gage to the teeth marks corresponding to the first wedge.

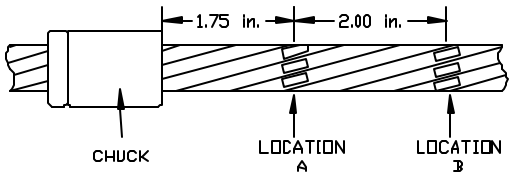

Figure 2.11 Location of Strain Gages for Strand 3, Test 2 and 3

Note that the strain data from the tests of strand 3 represent the most complete set of data. For various reasons many of the strain gages from tests of strand 1 and 2 were damaged or not functioning correctly. For this reason, only the data from strand 3 will be discussed in this section. Note that the strain data from the other tests are plotted in Appendix B. All the strains discussed in this section represent the change in strain due to bending; only initial strains due to the prestress force are not included. Note that the strains due to prestress from each of the gages were within 5% for each test.

Strain gages were placed on each of the outer 6 wires to monitor the response of the strand during bending. Figure 2.12 shows the variation of strain with mid-span deflection for a strand with a prestress force of 23.5 kip. The data are plotted such that increases in strain due to tension are positive.

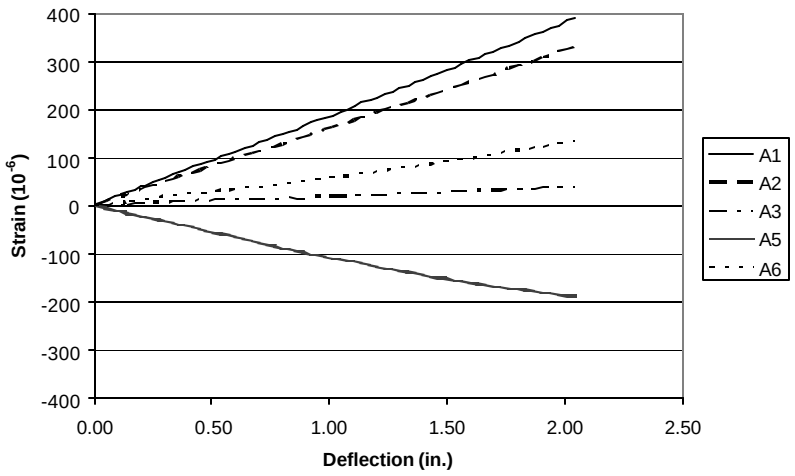

Figure 2.12 Strain Measured at Location A, Strand 3, Test 2

As expected, the strain gages attached to the extreme top and bottom wires experienced the highest absolute strains. Gages A1 and A5 were the furthest from the center of the cross section (Fig. 2.13). Note that the exact location of the

gages relative to the cross section was difficult to determine because the cross beams at the end of the frame prevented direct observation (Figure 2.7).

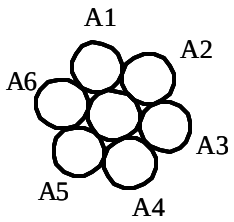

Figure 2.13 Approximate Location of Strain Gages at Location A for Strand 3, Test 2

It is important to note that the maximum strain measured by gage A1 is higher than the maximum strain measured by gage A5. This is because gage A1 was located almost directly below the centroid of the strand, while gage A5 was slightly off center of the centroidal axis. In addition, the strains are affected by the increase in tension during each test, so the measured strains are slightly higher than the actual bending strains. Similarly to the other tests, at least one of the strain gages did not adhere properly to the strand and data are not available for strain gage A4.

The data recorded at location B during the same loading cycle are plotted in Figure 2.14. The tensile strains increased in all gages at location B, although the magnitude of the variation was significantly less than that measured at location A. In tests of strands 1 and 2, it was shown that the bending strain in the strand is essentially zero approximately 12 in. from the face of the chuck, which agrees with the closed-form solution for a fixed end beam.

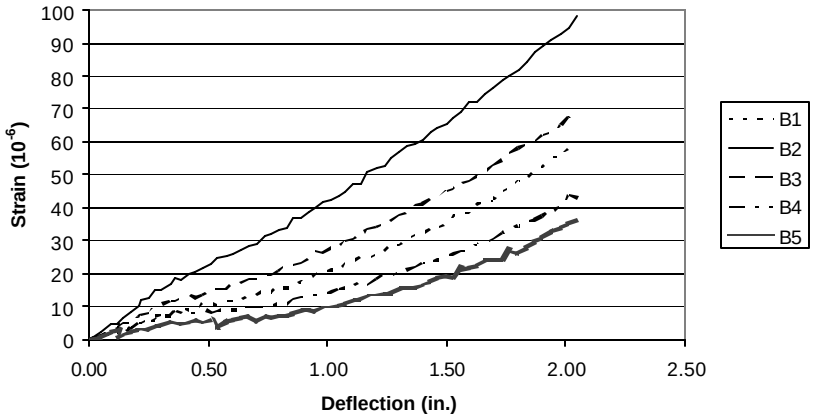

Figure 2.14 Strain Measured at Location B, Strand 3, Test 2

An interesting event that occurred frequently during the single-strand tests was that the measured strain did not return to zero after unloading of the specimen. The result is an apparent residual strain. Figure 2.15 shows one such example. Note that the apparent residual strain appeared for three of the five strain gages. The maximum residual strain in this example was 77 microstrain and occurred on strain gage A5. Possible sources are mechanics of the strand during bending or partial release of the strain gages, but the reason for the apparent residual strain was not positively identified.

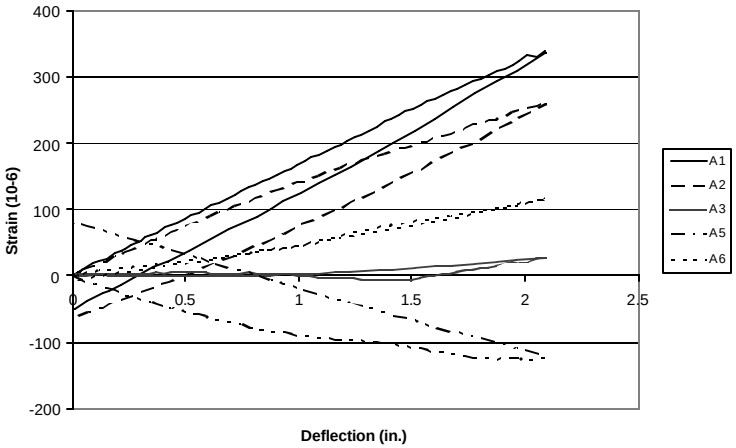

Figure 2.15 Strain Measured at Location A, Strand 1, Test 1 Showing Residual Strain

2.4 COMPARISON OF MEASURED AND CALCULATED RESPONSE

The measured response of the strands are compared with the expected response calculated using the closed-form solutions in this section. Two types of comparisons are discussed: stiffness of the strand and moments inferred from the measured strains. The stiffness from the closed-form solutions corresponds to an initial axial tension of 23.6 kip. In addition, the moment of inertia used in the closed-form solution corresponds to a solid section of the same area and shape as the 7-wire strand.

2.4.1 Stiffness Comparison

The average measured stiffness is compared with the stiffness calculated using the closed-form solutions in Table 2.3. As expected, the closed-form solutions bound the measured response of the strand. As stated earlier, the average measured stiffness of the strand is based on a linear least-squares approximation of measured data for six values of axial tension between 7.5 and 30.8 kip (Fig. 2.8).

Table 2.3 Stiffnesses of Closed-form Solution and Measured Response with a Prestress of 23.6 kip

	Stiffness (lb/in.)	Difference from Measured Stiffness (%)
Tests:	251	-
Simply-Supported:	241	-4.0%
Fixed End Solution:	257	2.4%

The actual moment of inertia of the strand is expected to be less than the moment of inertia of a solid section because the individual wires of a strand slip relative to each other as the load is applied. While it was not possible to measure the slip between wires, the effective EI of the strand can be estimated from the fixed end solution such that the measured and calculated strand stiffnesses are equal. Figure 2.16 shows the load-deflection curve for the fixed end solution and the measured response of a strand with a prestress force of 23.5 kip. Note that 23.5 kip was the closest to the desired level of 23.6 kip obtained during the single-strand tests. The fixed end solution is linear and can be described with Equation 2.13.

$$P = 256.8u_{\max} \tag{2.13}$$

where P is the transverse load and υ_{max} is the mid-span deflection. Note that the measured response is less stiff than the fixed end solution. This implies that wire slip did influence the bending response of the single strand.

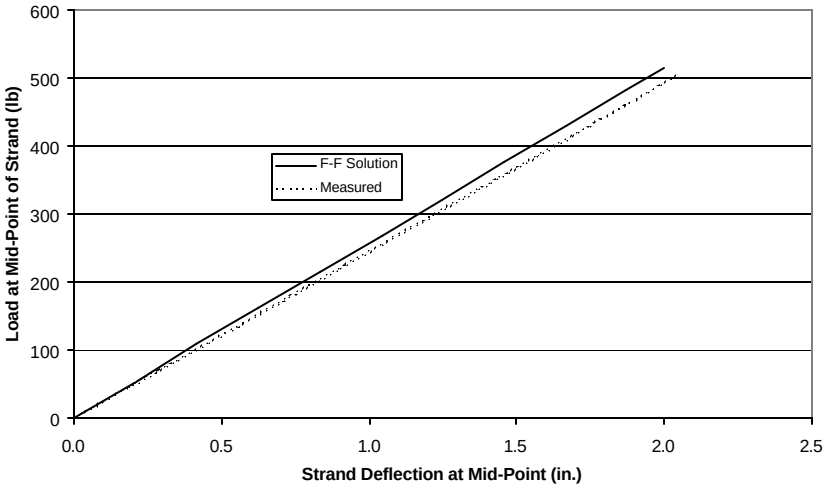

Figure 2.16 Comparison of Load-Deflection Curves for Test 2 of Strand 3 and the Fixed End Solution

The difference in stiffness between the fixed end beam solution and the measured results for test 2 of strand 3 is approximately 6%. In order for the observed response to match the fixed end solution an effective EI of 0.94EI should be used. Note that this effective EI is based on only one test.

An interesting thing to note is that the comparisons presented in this section are only applicable to single-strand bending. It is unknown how these results relate to the larger 19-strand tests. With the increased section size, the amount of wire slip could be significantly different. It is recommended that further testing be performed on multiple-strand specimens, with less than 19 strands, to define the relationship between the single-strand and 19-strand specimens.

2.4.2 Moment Comparison

Before the moments from the closed-form solutions can be compared with the measured data, moments must be calculated from the measured strain. The following assumptions were made to estimate moments from the strain data:

- The cross section of the strand is idealized as three separate layers and slip is ignored within each layer (Figure 2.17).
- The strain profile within each layer is assumed to be constant; however, the strains in adjacent layers are not equal.
- The strains in the top and bottom layers are assumed to be the maximum measured strains. The strain in the middle layer is calculated to satisfy equilibrium within the cross section.
- The longitudinal stress in the strand is related to the measured strain in the wires using Equation 2.13:

$$s = Ee\cos(f) \qquad (2.13)$$

where σ is the effective longitudinal stress in the strand, f is the orientation of the wires relative to the longitudinal axis of the strand (approximately 9°), ε is measured strain in the wires oriented along the axis of the wires, and E corresponds to the effective longitudinal modulus of the strand (28,000 ksi).

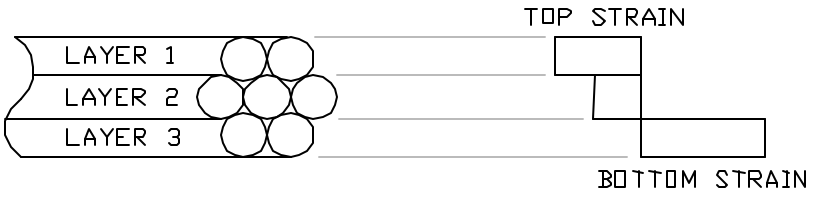

Figure 2.17 Cross-section Stress Diagram for a Single-Strand in Bending (ignoring prestress)

Moments were calculated at location A. During cycles 1 and 2 location A was approximately 2.5 in. from the face of the chuck. During cycles 3 and 4 location A was approximately 1.8 in. from the face of the chuck. The calculated moments are summarized in Table 2.4 and are compared with the moments calculated using the closed form solutions for the fixed end beam. The strains used to calculate the moments in Table 2.4 were obtained during a mid-span deflection of 2.0 in. The moments in the simply-supported beam are essentially zero near the ends, so these results are not included in the summary.

Table 2.4 Estimated Moments in Strand 3, Test 2 Compared with Closed-form Solution

	Distance from Chuck (in.)	Moment (lb-in)	Difference (%)
Fixed-Fixed Solution:	1.8	271	-
Fixed-Fixed Solution:	2.5	204	-
Test 2, Cycle 1:	2.5	196	4%
Test 2, Cycle 2:	2.5	200	2%
Test 2, Cycle 1:	1.8	241	11%
Test 2, Cycle 2:	1.8	241	11%

The moments calculated using the closed-form solution exceeded the moments inferred from the measured strains. Note that as the distance from the

face of the chuck increases, the difference between the moment and the fixed end solution decreases. One reason for this correlation is that slip between the wire layers increases with additional curvature. The relationship between the wire slip and curvature may be empirically estimated with more testing performed at other distances from the chuck. The empirical relationship between wire slip and curvature may be better understood with additional tests with multiple strands as discussed in Section 2.4.1.

2.5 SUMMARY

This chapter explains the development of closed-form solutions for a single 7-wire strand under tension and bending. In addition, closed-form solutions for a beam under tension and bending are used to bound the results of the tests. Based on the results, the following conclusions were made:

- The single-strand tests indicated that the strain due to bending is essentially zero at a distance of 12 in. from the face of the chuck, which agrees with the FEM model developed by Dowd (2001).
- When comparing the estimated average stiffness of the single-strand specimens, it was noted that the single-strand is approximately 2% less stiff than a fixed end classical model and approximately 4% more stiff than the simply-supported classical model. This concludes that the two models are upper and lower bounds to the actual stiffness of the strand.
- When comparing the fixed end beam solution to the results of test 2 from strand specimen 3, it was found that the fixed end solution was stiffer than the response of the strand. The difference in stiffness at 2.0 in. of deflection was approximately 6%. An effective EI of 0.94 EI

can be used to predict the response of a single strand using the fixed end beam solution. In addition, it was noted that the relation between the single-strand response and the 19-strand response is unknown with respect to wire slip.

- Based on the moment comparison between the single-strand tests and the closed-form solutions, it appears that the actual moment in the strand is between 2% and 9% less than the fixed end closed form solution. This indicates that the fixed end solution can be used for an adequate approximation of the single-strand specimens since the simply-supported solution has an end moment of zero.

CHAPTER 3
Strand Tension Fatigue Test

3.1 INTRODUCTION

Tension fatigue tests were conducted to establish the fatigue characteristics of the strand used to construct the first six, 19-strand stay cable specimens. This chapter describes the testing procedure, presents the results, and compares the results with specified design criteria and other published strand fatigue data. The results of the strand fatigue tests will be used by the research team to interpret the fatigue response of the stay-cable specimens. Specifically, the results will be used to determine if bending of the stay-cable specimens causes a reduction of fatigue life due to fretting or another mechanical interaction.

3.2 TEST PROGRAM

A total of twelve strand specimens were subjected to tensile fatigue loading. Each test was performed with an average stress of 104 ksi, the same tension as the prestress tension used in the bending fatigue tests. Stress ranges for the individual tests were 20, 30, and 40 ksi. The test specimens were subjected to cyclic loads with the prescribed stress range until at least one wire fractured or the number of cycles exceeded 6,000,000. Data from eight fatigue tests are used to evaluate the strand. Of the remaining four specimens, three tests ended prematurely when the strand failed within the grips and one specimen was inadvertently loaded to more than 95% of the guaranteed ultimate tensile strength before the fatigue loads were applied. The data from these tests are presented for completeness, but are not used to evaluate the strand.

3.2.1 Test Set-up

The tensile fatigue tests were conducted in a 200-kip MTS load frame. The testing machine consists of two heads, each of which contains a hydraulically controlled clamp. Each clamp can be used to apply lateral pressure to position a specimen within the test frame (Fig. 3.1). Once the clamp pressure is applied, the bottom head can be controlled to apply either static or cyclic tensile loads to a specimen.

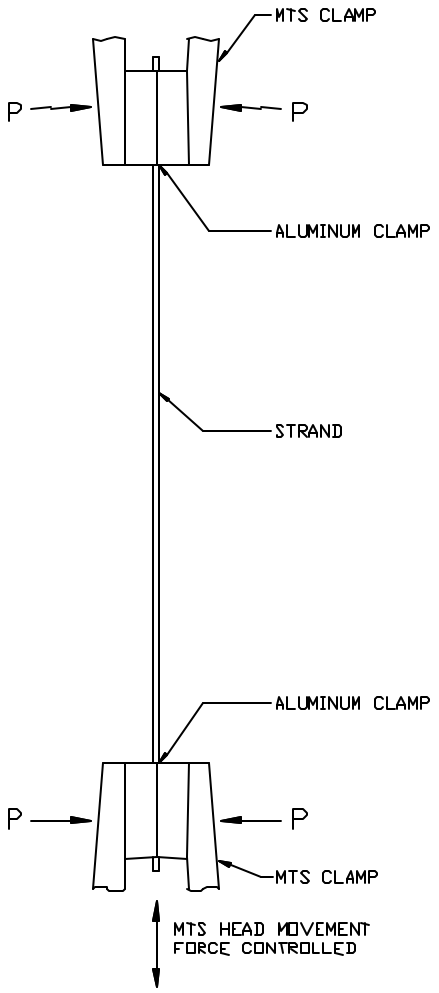

Figure 3.1 Schematic of Test Set-up

The cyclic loading was controlled using PC-based software developed by MTS (Test Star II). The load for each of the tests was applied using a load-controlled sine wave with feedback compensation. The feedback compensation corrects for errors between the input function and the actual motion of the test frame. The frequency of the load is also controlled by the software. In each test, the highest testing frequency possible was used. This frequency was limited by degradation of the sine wave function or inducing excessive dynamic motions in the test frame. Frequencies for the tests were between 1.5 and 4 Hz.

Each strand specimen was approximately 48" long from face-of-clamp to face-of-clamp. During installation special care was taken to position each specimen in the test frame vertically to minimize eccentricity. A special clamp system was developed so that the MTS grips could hold the strand without crushing the specimen. The aluminum clamps are discussed in the following section.

3.2.2 Aluminum Clamps

Aluminum clamps were built to hold the strand within the test machine grips. The aluminum clamps were designed based on recommendations by Lamb (1985). A general schematic of the clamp design is shown in Figure 3.2. Note that the dimensions of the clamp may be adjusted for different sized strand. Also, Lamb makes further recommendations to improve on the design shown below, but those modifications were not made because the simple aluminum clamp system worked well.

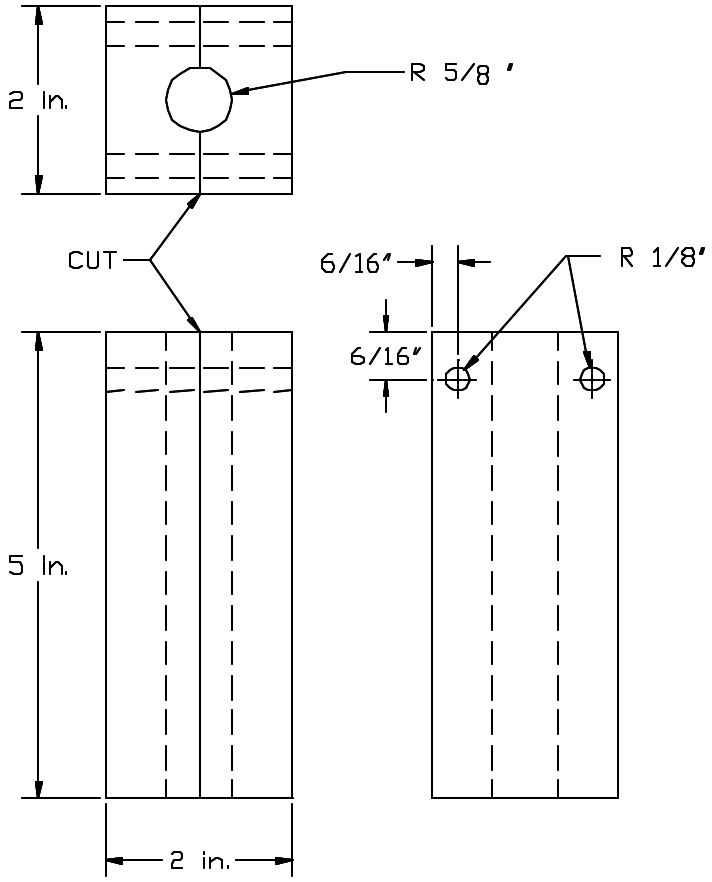

Figure 3.2 Schematic of Aluminum Clamp

The clamps were fabricated from a 5-in. long section of 2-in. square aluminum bar. A ? ”-diameter hole was drilled longitudinally through the center of the aluminum block. The hole was tapped approximately ? ” larger than the hole, providing a rough surface with which to grip the strand. Additional smaller holes are drilled near one end of the bar to hold the aluminum clamp on the strand before grip pressure is applied. The bar is then cut in half along the longitudinal axis (Fig. 3.2) and the strand is sandwiched between the two pieces of aluminum (Figure 3.3).

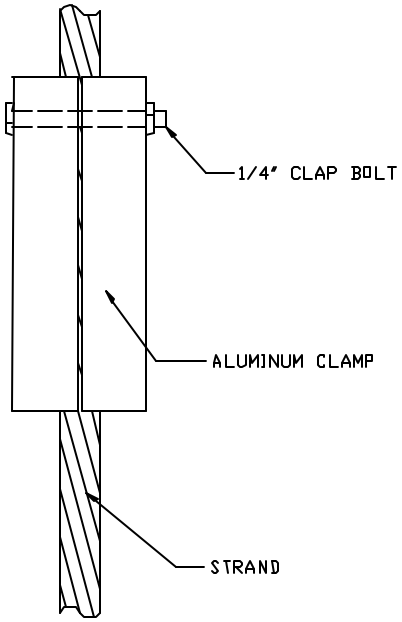

Figure 3.3 Aluminum Clamp in Position on Strand

As seen in Figure 3.4, when the grip pressure is applied to the aluminum clamps, the edges of the clamp come in contact with one another. The grip pressure must be controlled so that the aluminum does not crush. Figure 3.5 shows the inside surface of a clamp after testing. Note that the threads in the longitudinal hole allow the aluminum to conform to the shape of the strand. The lower modulus of the aluminum compared with that of the steel reduces the stress concentration at the clamp face which reduces the chance that a fatigue failure will occur near the grips. An attempt was made to reuse the aluminum clamps for more than one test, but the strand slipped through clamps that had been used previously. The results presented in this chapter refer only to tests using new aluminum clamps.

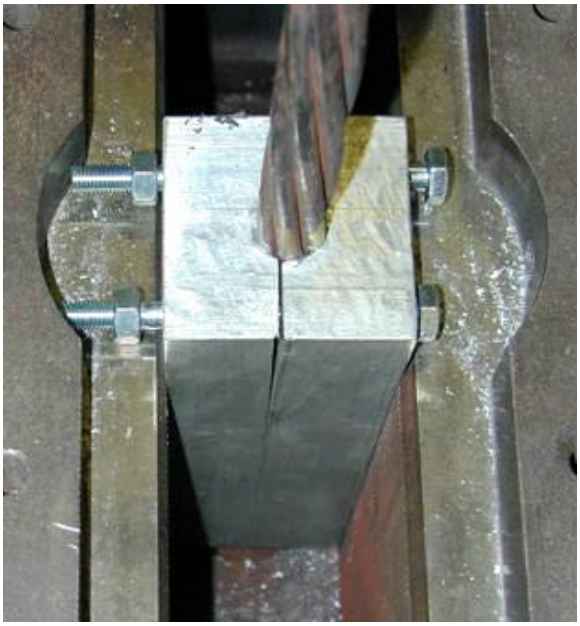

Figure 3.4 Aluminum Clamp under Pressure in MTS Grips

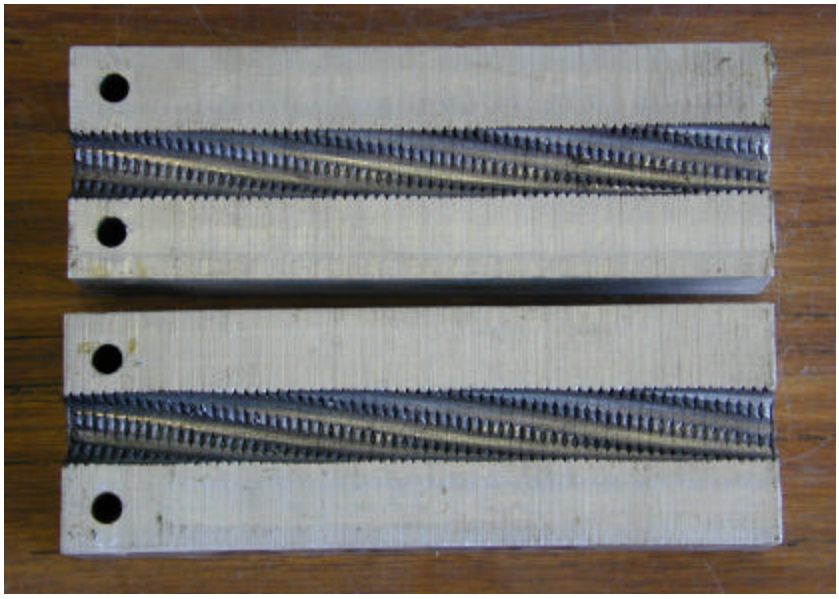

Figure 3.5 Photograph of Aluminum Clamp After Fatigue Test

3.3 RESULTS

The fatigue tests were performed at three different stress ranges: 20, 30, and 40 ksi. The stress range and number of cycles for each test is shown in Table 3.1. As stated previously, four specimens failed prematurely (2, 5, 7, and 11). The data from these tests are included in Table 3.1 for completeness, but are not used to evaluate the strand. The area used to calculate the strand stress was 0.2185 in^2 based on the manufacturer's specification sheet (Fig. B.16). The strand area was verified by researchers at UT (Fig. B.17).

Table 3.1 Single-strand Fatigue Test Results

Test No.	S_r (ksi)	N (cycles)	Notes
1	20	6,276,532	test stopped w/o failure
2	40	187,873	Grip Failure
3	40	365,353	
4	40	323,469	
5	40	145,098	Grip Failure
6	30	3,301,927	
7	30	90,942	Accidentally loaded to 265 ksi before test
8	30	1,009,600	
9	30	808,328	
10	40	232,773	
11	40	142,987	Grip Failure
12	30	848,521	

The results from the tests are compared with three other established strand fatigue standards: Paulson et al. (1983), PTI (1986), and PTI (2000). Tests described in Paulson characterize the fatigue life of ½-in., 270 ksi, low-relaxation strand. Paulson's test procedures were nearly identical to those used in this thesis. Paulson identified a mean fatigue life model (Eq. 3.1) and a lower bound relationship (Eq. 3.2):

$$Log(N) = 11.28 - 3.40 \cdot Log(S_r) \quad (3.1)$$

$$Log(N) = 11.00 - 3.50 \cdot Log(S_r) \quad (3.2)$$

Where N is the number of cycles and S_r is the stress range in ksi.

The Post-Tensioning Institute (PTI) specifies a lower limit for fatigue life for ASTM A416 uncoated, seven-wire, low-relaxation strand used to construct stay cables (PTI 2001 and 1986). For comparison, the results of the tensile fatigue tests are compared with the PTI specifications for 1986 and 2001. The reason for providing both the 1986 and the 2001 PTI specifications is that there is a significant difference between the fatigue requirements for the two editions. For the same given minimum number of cycles, the 1986 PTI specification requires a lower stress range than the requirements in the 2001 PTI specification. The 2001 stress ranges are between 14 and 16 percent higher than the 1986 stress ranges. Another interesting note is that while fatigue requirements for individual strands increased between the 1986 and 2001 specification, other related design limits did not change. The maximum allowable stress range for assembled stay cables remained unchanged and the assembled stay cable fatigue test stress range did not change. It is the research team's understanding that the 1986 PTI specification was based on the results of Paulson's data. The basis for the 2001 PTI strand fatigue requirements is currently unknown.

Both PTI Specifications require that the maximum stress in each cycle be 0.45 f'_s (121.5 ksi), where f's is the guaranteed ultimate tensile strength. In each of the tests described in this report, the average stress was 0.4 f'_s (108 ksi) and the maximum stresses were 0.44 f'_s, 0.46 f'_s, and 0.47 f'_s for the 20, 30, and 40 ksi tests respectively. So the PTI test procedures and the test procedures used in this

thesis were nearly identical. The 1986 and 2001 PTI specification requirements are summarized in Table 3.2.

Table 3.2 PTI Specification Strand Fatigue Requirements

No. of Cycles	2001 PTI Test Stres Range (ksi)	1986 PTI Test Stres Range (ksi)	% Decrease
2,000,000 +	30.9	26.0	15.9%
2,000,000	33.1	28.0	15.4%
500,000	43.8	37.5	14.4%
100,000	64.3	55.0	14.5%

The test data are plotted in Figure 3.6. The lower bound and mean relationship developed by Paulson and the PTI minimums are plotted. The majority of the measured data fall between the mean and lower bound reported by Paulson. This indicates that the strand had lower than average strength relative to the sample population of strand that Paulson tested. In addition, the majority of the tests also fell below the minimums set by the PTI specifications. It is important to note that while only strand test number 1 satisfied the 2001 PTI specification, strand test numbers 1 and 6 satisfied the 1986 specification. In conclusion, the overall results indicate that the strand used in the full-sized specimen tests have a lower than average fatigue life and do not satisfy either the 1986 or the 2001 PTI specifications.

It is recommended that further testing be performed on the strand to construct the 19-strand specimens 1 through 6 to verify these results. In addition, the PTI governing body should be contacted to verify the source of the 2001 PTI strand fatigue requirements. If the 2001 fatigue requirements are correct, it may be very difficult to obtain strand that satisfy the specification. It is also

recommended that strand used to construct future 19-strand specimens should be tested in a similar manner and compared to the results presented in this thesis.

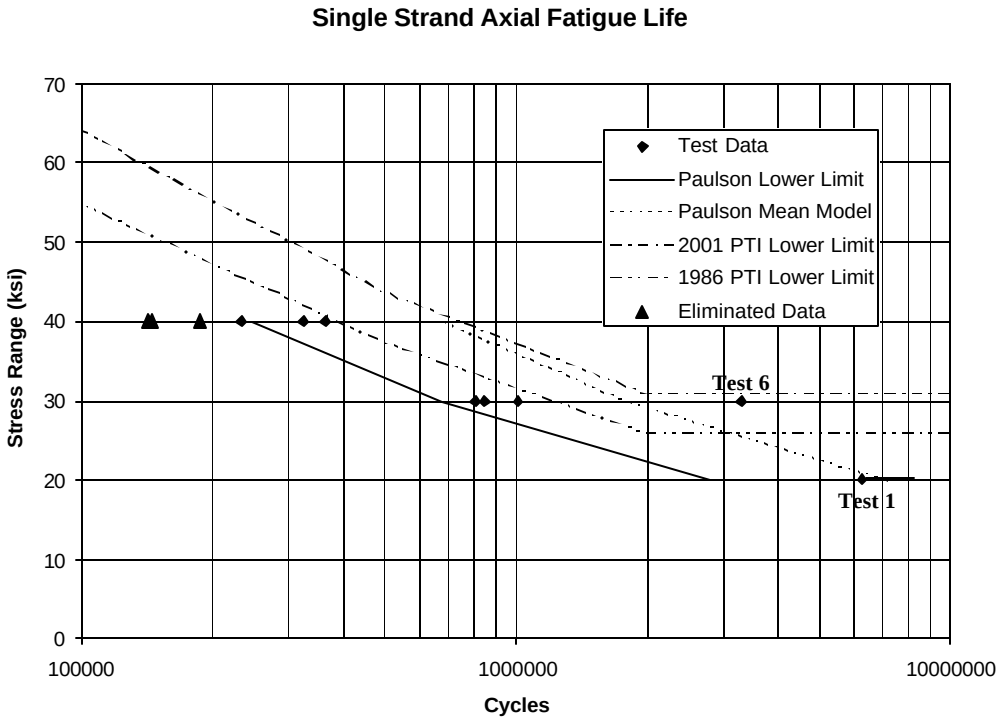

Figure 3.6 Tensile Fatigue Test Results

Note that Test 1 was stopped at 6,276,532 cycles without failure. This is indicated with an arrow in Figure 3.6.

CHAPTER 4
Characterization of Cable Vibration Data from the Fred Hartman Bridge

4.1 INTRODUCTION

Researchers from Johns Hopkins University (JHU) instrumented the Fred Hartman Bridge stay cables with accelerometers in October 1997. In this chapter, the data from the accelerometers are used to characterize the motion of the stay cables and estimate the number of wind-rain induced vibration cycles that each cable has experienced since construction in September 1995.

The measured acceleration data are integrated numerically to calculate the displacement response of each cable. Displacement histories are then used to characterize the motion of the cables in terms of frequency, primary mode of vibration, and maximum modal displacement. A rain-flow algorithm is then used to count the number of displacement cycles experienced during each wind-rain event.

The results of the rain-flow analyses are then used to develop an equivalent displacement and calculate the average number of cycles per minute for each cable. Next, the statistical data compiled by researchers at JHU are used to estimate the amount of time that each of the cables has undergone wind-rain induced vibrations. The estimated total number of cycles that each cable has experienced is then compared with the observed fatigue life of the first five stay cable specimens. After further cable stay testing, the research team should be able to use the results of the cable fatigue characterization and the cable stay tests

to estimate fatigue damage and the remaining life of the stay cables that support the Fred Hartman Bridge.

4.2 DATA

Researchers from JHU University instrumented and began collecting data on the Fred Hartman Bridge in October 1997. Instrumentation includes 19 two-axis accelerometers attached to the stay cables and a data acquisition system (DAQ) with a sampling frequency of 40 Hz. The DAQ continually monitors each transducer and saves the data to a disk whenever predetermined wind speed or cable acceleration thresholds are exceeded. Each time the predetermined thresholds are exceeded, the DAQ saves data for 5-minutes (Main et al. 2000). Data received from JHU include a statistical database of all the records obtained since instrumentation was installed and ten files, each with the acceleration histories for seven different cables during wind-rain events. For each cable, the acceleration history includes acceleration in two perpendicular planes.

4.2.1 Statistical Database

Researchers at JHU compiled a database of statistical information for each 5-minute record obtained since the Fred Hartman Bridge was instrumented in October of 1997. Each record was divided into one-minute segments and statistical data were calculated for each segment. This database is used to estimate the number of times each cable experienced wind-rain induced vibration. The following statistics were compiled for each one-minute segment:

- Maximum displacement (measured and modal)
- Primary vibration modes
- Rainfall and rate of rainfall during event
- Wind speed and direction
- Date and time of each record

- Other information not applicable to this report

Note that the DAQ system thresholds were set so that all the vibration events that occurred while rain was falling were recorded. The vast majority of the recordings are not large amplitude events such as wind-rain events, but are small amplitude events. For this reason, wind-rain induced vibrations must be identified within the database using some statistical criteria. The statistical criteria used here is maximum displacement. The displacement criteria and the development of the criteria are discussed in Section 4.4.1.

4.2.2 Acceleration Histories for Seven Cables

Researchers at JHU also provided the research team with ten sets of acceleration histories from wind-rain induced vibration events. Each file consists of a 5-minute acceleration time history with two axes of acceleration from seven separate cables on the Fred Hartman Bridge (14 records in total). The cables included in the records their associated lengths, and the location of the accelerometers on each cable is listed in Table 4.1. AS<u>X</u> indicates a cable on the south bridge tower and AN<u>X</u> indicates a cable on the north bridge tower. For example, AS1 is the 1st cable (from south to north) on the west side of the south towers. All the instrumented cables are located on cable plane A (Fig. 4.2).

Table 4.1 Cable Identification and Lengths

Cable Identification	Length (ft)	Location of Accelerometer (ft)*
AS1	564	51
AS5	448	52
AS9	285	37
AS16	286	38
AS23	599	65
AS24	647	60
AN24	647	63

* Measured from Deck Anchorage

For each cable, a separate record exists for each axis of the two-axis accelerometers. The axes are identified as in-plane or out-of-plane. In-plane indicates that the acceleration is in the plane of the cables and out-of-plane indicates that the acceleration is perpendicular to the plane of the cables. Figures 4.1 and 4.2 identify the in-plane and out-of-plane directions and the cable identification scheme for the south bridge tower. Note that the cables are not in a vertical plane, but they are all within a single plane (Fig. 1.2). For conciseness, the out-of-plane direction is called the lateral direction for the rest of this report.

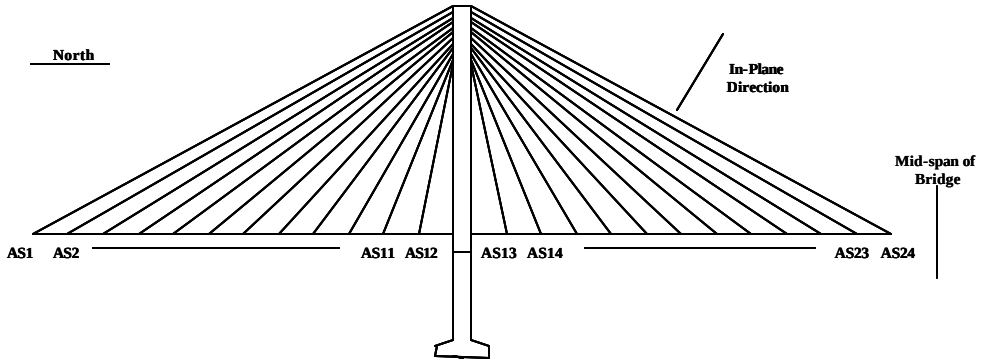

Figure 4.1 Schematic of South Tower Profile View

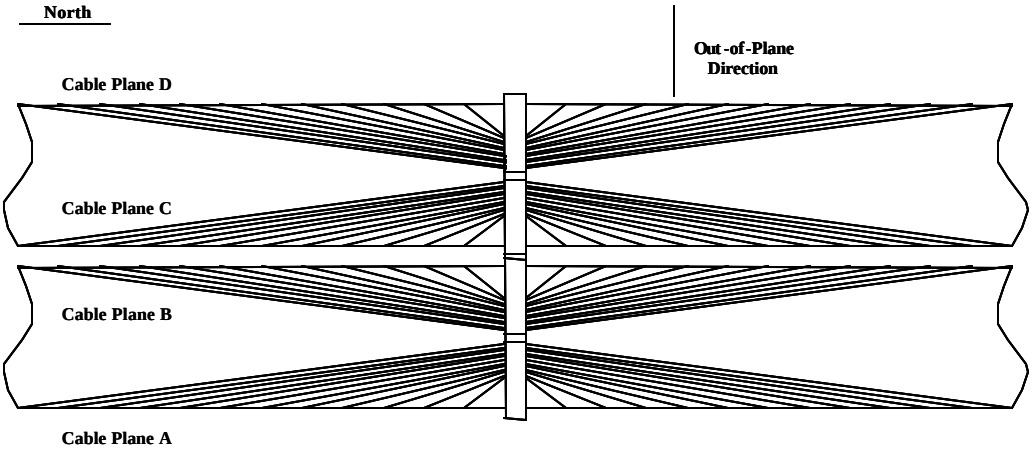

Figure 4.2 Schematic of South Tower Plan View

Figure 4.3 shows a representative example of a 15-second acceleration history of one axis of cable AS9 during a wind-rain event.

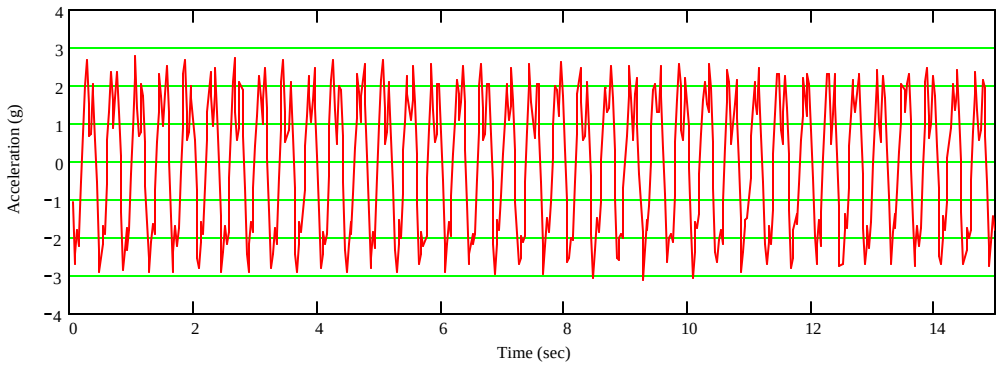

Figure 4.3 Acceleration-time Record for Cable AS9

4.2.3 Integration of Acceleration Histories

The acceleration data from the ten wind-rain induced vibration files were used to calculate velocity and displacement records using numerical integration. There were some challenges involved with numerical integration of the measured acceleration. First, a small offset was identified in most of the acceleration records. The offset can be seen in records when the signal is not centered about zero acceleration. Note that a constant error in the acceleration record becomes a linear error in the velocity record and a quadratic error in the displacement record. Over a five-minute duration even a small offset in the acceleration record becomes significant in the resulting displacement signal. This issue was overcome by subtracting a running average from each data point (Equation 4.1). The running average was calculated using data adjacent to each data point. Correcting the acceleration record with this method creates a record that is centered about zero without changing any other important parameters of the record. It was found that a running average of approximately 21 points was

effective in eliminating the offset. Note that a running average was used as opposed to an overall average because it was not definite that each offset was constant.

$$a_i = a_i - \frac{\sum_{n=i-10}^{i+10} a_n}{21} \qquad (4.1)$$

,where a_i is an arbitrary data point.

Next, the acceleration signals contain low-frequency noise components that can overpower the high-frequency signal which represents the response. This issue can be addressed by using a high-pass filter to eliminate the low-frequency noise (Hudson 1979). The filter used in this research was a high-pass, 5^{th} order, Butterworth filter. Based on recommendations from researchers at JHU, a cutoff frequency equal to half the natural frequency was used (Main et al. 2000). This filter and cutoff frequency were found to be effective at eliminating the low-frequency noise without distorting the useful high-frequency components (Main et al. 2000). Figure 4.4 shows a calculated velocity history before adjustment. Figure 4.5 shows the same record after subtracting a running average and filtering. Note that after integration of the raw acceleration record, the constant offset created an unusable velocity record. With smoothing and filtering the velocity record is centered at zero and only includes the high frequency signal which represents vibration of the stay cables. The results of the filtering are difficult to notice in Figures 4.4 and 4.5.

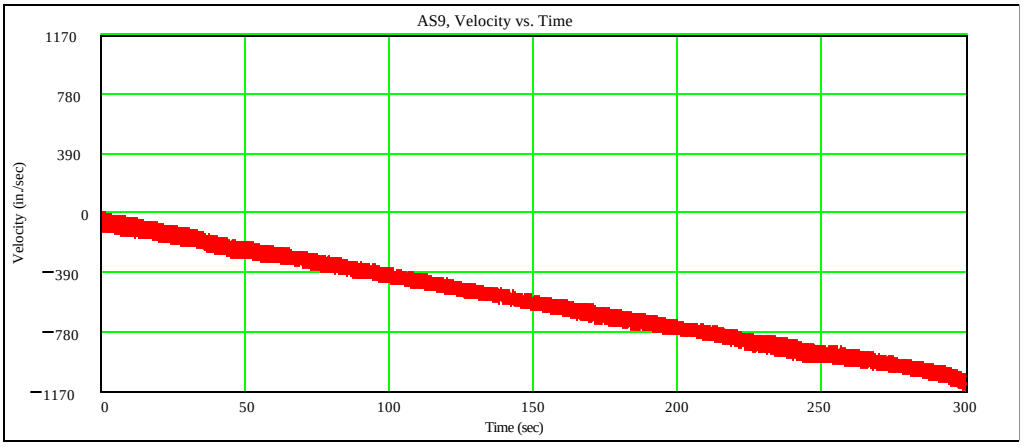

Figure 4.4 Velocity Record for Cable AS9 without Filtering or Smoothing

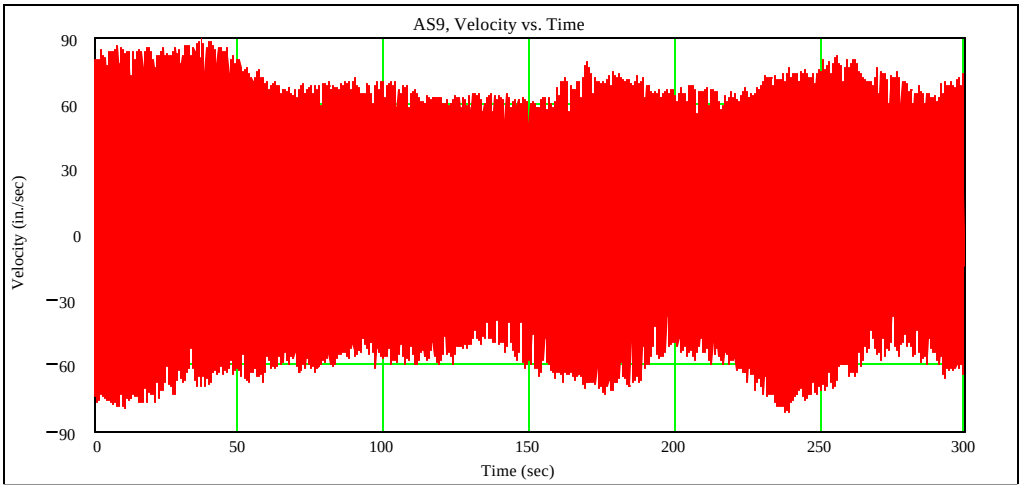

Figure 4.5 Velocity Record for Cable AS9 with Filtering and Smoothing

The procedure used to obtain a displacement record from an acceleration record is as follows:

- Smooth the original acceleration record by subtracting a running average.
- Use a high-pass filter to remove the low-frequency noise from the acceleration record.
- Numerically integrate the acceleration record to obtain velocity.
- Use a high-pass filter to remove the low-frequency noise from the velocity record.
- Numerically integrate the velocity record to obtain displacement.
- Use a high-pass filter to remove the low-frequency noise from the displacement record.

It is important to note that the accelerometers used on the Fred Hartman Bridge cables have a maximum range of ± 4g. In most records of large amplitude vibration, the 4g limit was exceeded by some of the cables. This resulted in saturation of the signal. The entire records were included in the displacement analysis to obtain the maximum measurable displacement. Note that while the maximum displacement from a saturated record is lower than actual displacement, it will at least provide an estimate of the displacement amplitude. Recommendations for further research include instrumentation using accelerometers with a larger range.

The procedure used to calculate the final displacement record was developed primarily by researchers at Johns Hopkins. In order to verify that the procedure did not significantly alter the resulting displacement ranges and vibration frequencies, the calculated displacement of a filtered record was compared to the calculated displacement of an unfiltered record. After further investigation, it was discovered that filtering of the records did not significantly change the overall displacement record and there was no difference when the

maximum displacements were occurring. In addition, the displacement ranges were not noticeably altered. This was confirmed by comparing the rainflow cycle counting results of the filtered and unfiltered displacements. This is important because the displacement range is the controlling factor the fatigue analysis presented in this thesis. Rainflow cycle counting is explained in Section 4.3.

4.2.4 Characterization of Motion

After obtaining displacement records for each of the cables, the cable motions were analyzed. First, the in-plane and lateral displacement signals were plotted against each other to obtain a Lissajous diagram for each record (Fig. 4.6). Figure 4.6 shows a displacement signal from Cable AS9 for 1 second of motion and does not correspond to a time of maximum displacement. The Lissajous diagrams were created to verify that the cable vibrations existed in both planes.

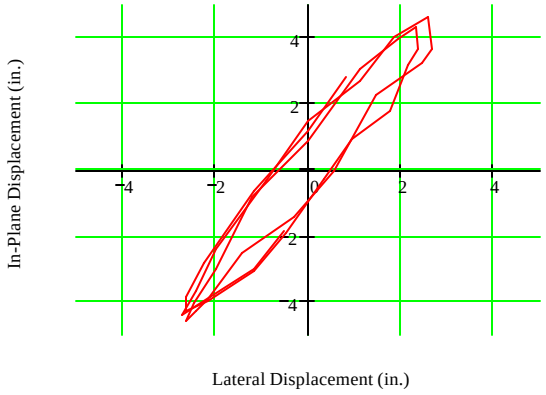

Figure 4.6 Lissajous Diagram of Cable AS9 for 1 Second of Time

Because the overall displacement of each cable does not occur in only the in-plane or lateral direction, the total displacement record was calculated for each cable by vector addition of the displacement. Table 4.2 provides the maximum displacement calculated at the location of the accelerometer for each cable during

each event. The file numbers correlate to the date the file was recorded. The first 8 numbers represent the year, month, and day respectively that the file was recorded. The last one or two digits corresponds to the number of the recording on that date. For example file number 1997100111 is the 11th file recorded on October 1, 1997. The in-plane and lateral signals were combined by using Equation 4.2:

$$D_{total} = \sqrt{D_{ip}^2 + D_{lat}^2} \qquad (4.2)$$

Where D_{total} is the total displacement of the cable at the accelerometer location, D_{ip} is the displacement in the in-plane direction, and D_{lat} is the displacement in the lateral direction. Note that the location of the accelerometer on each cable is provided in Table 4.1.

Table 4.2 Maximum Displacements at Accelerometer Locations (in.)

	Cable Identification						
File No.	**AS1**	**AS5**	**AS9**	**AS16**	**AS23**	**AS24**	**AN24**
1997100111	0.34	0.43	1.07	8.90	12.67	8.01	2.83
1997100628	0.09	0.29	0.15	2.96	5.23	3.69	0.52
199710071	11.73	11.13	8.37	0.77	0.91	2.47	8.74
1997100713	9.33	8.36	10.05	1.11	1.28	2.61	7.11
1997112880	0.13	0.89	0.54	10.12	2.98	0.87	0.53
1997120718	7.51	11.87	10.97	1.18	1.92	3.46	8.99
1997120746	6.94	16.95	11.36	1.30	3.67	2.78	9.18
1998062816	0.68	0.04	0.04	10.48	13.40	12.11	2.64
1998062818	0.39	0.01	0.06	8.94	12.03	9.07	2.60
199807038	0.24	0.01	0.00	5.43	4.77	6.68	12.34

Frequency content of the total displacement records was determined using a Fast Fourier Transform (FFT). Frequencies corresponding to the five highest peaks in the FFT were recorded, which correspond to the frequencies of the modes that dominate the displacement response. Note that the mode with the highest amplitude in the FFT of the displacement record may not be the same as

the modes with the highest amplitude in the FFT of the acceleration response. Acceleration amplitude may be a misleading indicator of actual vibration amplitude because participation of the higher frequency components is exaggerated in the acceleration records (Main 2000).

Once the five dominant frequencies were identified, the modes in which each cable was vibrating were identified. The mode number can be obtained using Equation 4.3:

$$i_m = \frac{F_D}{F_n} \tag{4.3}$$

,where i_m is the vibration mode number, F_D is the dominant frequency of the displacement response, and F_n is the measured natural frequency of the cable. Table 4.3 provides the natural frequencies for the stay-cables (Poston 1990).

Table 4.3 Measured Natural Frequency of Stay-Cables

Cable	Natural Frequency (Hz)
AS1	0.668
AS5	0.810
AS9	1.255
AS16	1.263
AS23	0.654
AS24	0.585
AN24	0.585

Table 4.4 shows the primary mode of vibration for each cable during each event. Note that not all of the cables experienced large-amplitude vibrations during every event. However, each cable did undergo at least some small vibration during each event. These low-level vibrations are most likely attributed to vortex shedding. Each vibration event with a maximum displacement more

than 3.0 in. is highlighted in Table 4.4. The location of the each accelerometer and all the primary mode shapes for each cable are provided in Figure 4.7. Note that all the accelerometers are located before the maximum amplitude of any of the mode shapes.

Table 4.4 Primary Vibration Mode of Cables

	Cable Identification						
File No.	**AS1**	**AS5**	**AS9**	**AS16**	**AS23**	**AS24**	**AN24**
1997100111	3	4	2	**2**	**5**	**5**	5
1997100628	4	4	2	2	**5**	5	5
1997100710	**2**	**3**	**2**	2	4	3	**4**
1997100713	**3**	**3**	**2**	2	3	3	**3**
1997112880	4	3	2	**2**	3	3	3
1997120718	4	**3**	**3**	2	3	**4**	**3**
1997120746	**3**	**3**	**2**	2	**4**	4	**4**
1998062816	**3**	3	2	**2**	**3**	**5**	4
1998062818	4	3	2	**2**	**3**	**5**	5
1998070380	2	3	2	**2**	**4**	**3**	**3**

Figure 4.7 Accelerometer Locations vs. Possible Mode Shapes

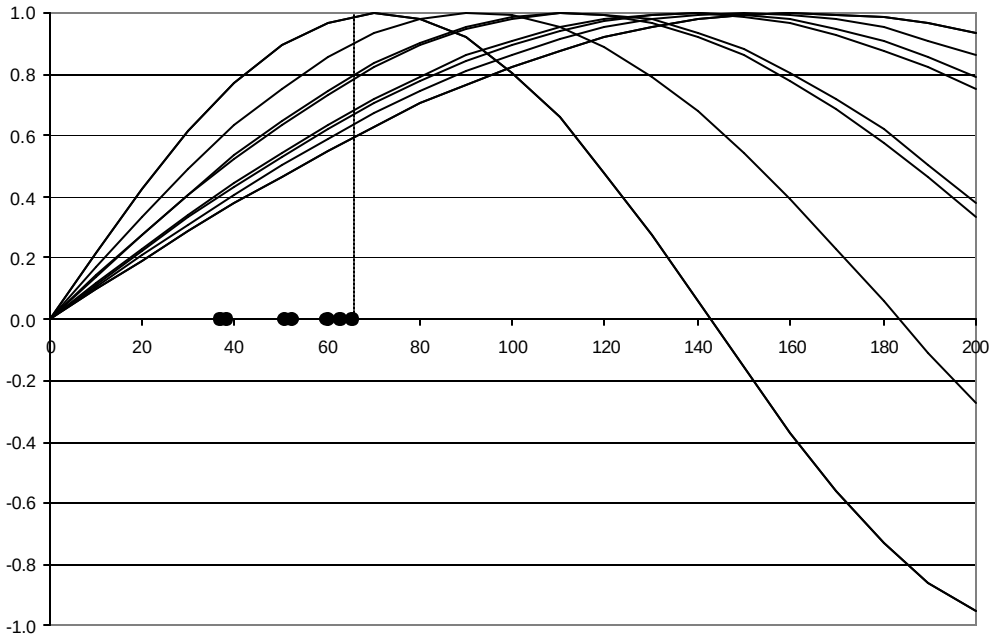

4.3 RAIN-FLOW ANALYSIS

As in any measured response, the amplitude of the cycles is not constant. Therefore, some type of cycle counting scheme must be employed to reduce the irregular displacement history into a series of constant amplitude events (Downing et al., 1982). Rainflow cycle counting may be used for this purpose. Several other algorithms are available to perform cycle counting; however, rainflow counting is commonly used in fatigue analyses. The result of a rainflow analysis is a matrix providing the number of cycles in various ranges of displacement, strain, stress, or other parameter.

Fatigue damage is commonly related to stress range and not the mean or maximum stress. For the cables studied in this project, the research team has not been able to measure stress or strain directly from the test specimens or the bridge cables. As a result, this report uses the displacement at the location of the accelerometer to describe the number of displacement cycles experienced by each cable. It is anticipated that other researchers on this project will be able to relate this displacement to stress near the anchorage, after further refinement of the finite element models.

4.3.1 Rainflow Algorithms

The most commonly used algorithm for rainflow analysis is published in ASTM E 1049. The program that was utilized for this project is called CRUNCH. It is a statistical program for fatigue analysis developed at the National Wind Technology Center (Buhl 2002). Rainflow cycle counting is one of many functional options included in the program. To verify the validity of the rainflow cycle counting algorithm used by CRUNCH, the results of the program were compared to the results of a program written according to ASTM E 1049. The differences identified between the results of the two programs were minor and

considered insignificant. For this reason and because CRUNCH has a user-friendly interface, it was used to perform all the rainflow analyses described in this report.

4.3.2 Rainflow Analysis Results

The results of the rainflow analyses include the number of cycles for a set of predetermined displacement ranges for each cable in each record. An example of a rainflow counting output is provided in Table 4.5. Each displacement range is called a bin. Each bin in Table 4.5 is 1.0 in. except the first bin which is only 0.5 in. The number of cycles counted for each bin is provided for each cable. Note that for each cable, the cycle counts for each bin are given as cycles/time. In all the rainflow analyses performed for this thesis the amount of time is 5 minutes.

Table 4.5 Rainflow Results for File No. 199710010

Displacement Range (in)		AS1 (cyc/time)	AS5 (cyc/time)	AS9 (cyc/time)	AS16 (cyc/time)	AS23 (cyc/time)	AS24 (cyc/time)	AN24 (cyc/time)
0.0	0.5	425	3	1	1310	723	1059	468
0.5	1.5	45	0	0	41	200	46	61
1.5	2.5	35	0	0	0	118	0	79
2.5	3.5	27	1	0	0	47	0	68
3.5	4.5	25	3	0	0	9	0	52
4.5	5.5	27	3	0	0	0	0	58
5.5	6.5	24	10	0	0	0	0	46
6.5	7.5	28	13	0	0	0	0	21
7.5	8.5	24	21	12	0	0	0	10
8.5	9.5	52	28	81	0	0	0	22
9.5	10.5	46	39	135	0	0	0	29
10.5	11.5	47	51	164	0	0	0	30
11.5	12.5	38	44	153	0	0	0	22
12.5	13.5	24	55	95	0	0	0	19
13.5	14.5	26	69	71	0	0	0	2
14.5	15.5	20	94	33	0	0	0	0
15.5	16.5	5	86	2	0	0	0	1
16.5	17.5	1	85	0	0	0	0	0
17.5	18.5	1	66	0	0	0	0	0
18.5	19.5	0	47	0	0	0	0	0
S(cyc/time) :		920	718	747	1351	1097	1105	988

From the results, it is evident which cables were experiencing both wind-rain induced vibration and other low amplitude vibrations. During the low amplitude vibrations, the cable undergoes very small displacements for a very large number of cycles. During a wind-rain event, the cable undergoes larger displacements and significantly fewer cycles. Because only the wind-rain induced vibrations are important for this report, a threshold had to be established to distinguish between the two types of vibrations. After review of the rainflow analysis for each displacement record, it was noted that most of the cables appeared to have a threshold between 3 and 5 in. An example of this phenomenon can be seen in Table 4.5. In Table 4.5, cables AS5 and AS9 have only large displacements because they were experiencing only wind-rain vibrations. Cables AS16, AS23 and AS24 have only small displacements because they were not experiencing wind-rain vibrations. Cables AS1 and AN24 have both small and large displacements because they were experiencing wind-rain vibrations for only a portion of the record.

To be conservative, a threshold of 3 in. was used to distinguish between wind-rain induced vibrations and small amplitude vibrations. An example of rainflow results without the bins smaller than 3 in. is provided in Table 4.6. The following sections discuss analyses using only the results from bins with a midpoint of 3 in. or greater. The summarized results of the rainflow analysis for each displacement record are presented in Appendix C.

Table 4.6 Rainflow Results for File No. 199710010 without Bins Smaller than 3 in.

Displacement Range (in)		AS1 (cyc/time)	AS5 (cyc/time)	AS9 (cyc/time)	AS16 (cyc/time)	AS23 (cyc/time)	AS24 (cyc/time)	AN24 (cyc/time)
2.5	3.5	27	1	0	0	47	0	68
3.5	4.5	25	3	0	0	9	0	52
4.5	5.5	27	3	0	0	0	0	58
5.5	6.5	24	10	0	0	0	0	46
6.5	7.5	28	13	0	0	0	0	21
7.5	8.5	24	21	12	0	0	0	10
8.5	9.5	52	28	81	0	0	0	22
9.5	10.5	46	39	135	0	0	0	29
10.5	11.5	47	51	164	0	0	0	30
11.5	12.5	38	44	153	0	0	0	22
12.5	13.5	24	55	95	0	0	0	19
13.5	14.5	26	69	71	0	0	0	2
14.5	15.5	20	94	33	0	0	0	0
15.5	16.5	5	86	2	0	0	0	1
16.5	17.5	1	85	0	0	0	0	0
17.5	18.5	1	66	0	0	0	0	0
18.5	19.5	0	47	0	0	0	0	0
S(cyc/time) :		415	715	746	0	56	0	380

4.4 ESTIMATED FATIGUE DAMAGE

4.4.1 Equivalent Displacements

In order to estimate the amount of fatigue damage caused by wind-rain induced vibrations, the rainflow results need to be related to the results from the 19-strand, grouted fatigue tests described in Chapter 2. In the grouted fatigue tests, the displacement range was constant throughout each test. To relate the test data to the measured displacement data, Miner's Rule is used to convert the rainflow results to a single equivalent displacement for each cable during each event (Table 4.7). Miner's Rule is given in Equation 4.4:

$$D_{re} = \sum_i \left(g_i \cdot D_{ri}^3 \right)^{1/3} \qquad (4.4)$$

,where D_{re} is the equivalent displacement and D_{ri} is the midpoint of each displacement bin. γ_i is the proportion of the number of cycles in bin i to the total number of cycles in all the bins and is calculated using Equation 4.5:

$$g_i = \frac{(cycles/time)_i}{\sum_i (cycles/time)_i} \tag{4.5}$$

Table 4.7 Equivalent Displacements for each Cable During each Wind-Rain Vibration Event

File	AS1	AS5	AS9	AS16	AS23	AS24	AN24
1997100111	8.5	13.5	13.6	--	4.3	--	8.5
1997100628	10.7	10.5	12.5	--	4.0	--	8.2
1997100710	10.6	14.8	11.7	--	4.0	--	8.7
1997100713	--	--	--	4.1	4.9	6.9	--
199711288	--	--	--	9.0	10.2	16.0	4.1
1997120718	--	--	--	6.8	8.7	6.1	13.4
1997120746	--	--	--	11.9	--	4.3	--
1998062816	--	--	--	9.6	11.0	11.5	4.6
1998062818	--	--	--	15.1	14.7	17.7	4.0
199807038	17.9	19.7	19.4	--	5.0	6.6	12.3

Once the equivalent displacement amplitude for each cable during each event was obtained, Miner's Rule was used again to obtain the overall equivalent displacement for each cable from all the events combined. To do this the equivalent displacement for each event was used for D_{ri} and the number of cycles for each event was used for $(cycles/time)_i$ in Equations 4.4 and 4.5 respectively. The over all equivalent displacement for each cable is provided in Table 4.8.

In addition to the equivalent displacement, the number of cycles that each cable experiences during a wind-rain event is needed to define the fatigue damage. To estimate the number of cycles associated with each equivalent displacement, the average cycles/minute for each cable during each wind-rain

vibration event was calculated. The average number of cycles/minute for each cable is also provided in Table 4.8.

Table 4.8 Overall Equivalent Displacements and Average Cycles per Minute for each Cable

	AS1	AS5	AS9	AS16	AS23	AS24	AN24
D_{re}:	9.4	12.1	11.5	11.1	11.6	13.4	7.9
Cycles/min:	33	64	58	70	53	55	41

4.4.2 Estimated Fatigue

To estimate the fatigue damage to the cables due to wind-rain induced vibration, the overall equivalent displacement for each cable is assumed to be applied to the cable at the associated cycles per minute during each wind-rain vibration event. The number of events and length of each event that each of the cables has undergone is estimated using the JHU database. The length of each event is conservatively estimated at one minute. One minute is the estimate since it is the length of each of the records used to create the statistics in the JHU database and hence it is the maximum possible length of each of the events. The database has 163,230 records from October 30, 1997 to December 13, 2002. The number of events is extrapolated to include all the time since the bridge was constructed in September of 1995.

However, the DAQ system used to record each record was not operational during the entire period. For that reason, the estimate for the number of cycles may actually be low and should be increased a reasonable amount to ensure a conservative estimate. Based on the number of times that the instrumentation on each cable was discovered to be inoperative, a The total number of cycles estimated for each cable is increased by certain percentage

based on the number of times the instrumentation on each cable was inoperable between October 30, 1997 and December 13, 2002. Table 4.9 shows the number of events from the database and the resulting number of cycles for each of the cables analyzed.

Table 4.9 Total Number of Wind-Rain Cycles for Each Cable

	AS1	AS5	AS9	AS16	AS23	AS24	AN24
No. of Events:	779	4,182	1,551	1,103	1,103	410	410
Cycles/Min.:	33	64	58	70	53	55	41
Total Cycles:	26,027	269,316	90,689	77,534	58,895	22,548	16,702
Increase by:	29%	12%	18%	12%	6%	6%	6%
Adjusted Total Cycles:	33,575	301,634	107,013	86,838	62,429	23,901	17,704

4.5 COMPARISON WITH TESTS

So far in the 19-strand grouted tests, less than 2% of the wires had failed at the anchorage after 500,000 cycles (Poser 2002). Table 4.10 provides a summary of the number of cycles until the first wire break for the first five 19-strand specimen. For comparison, Table 4.11 provides a summary of the estimated fatigue of the Fred Hartman stay-cables. In both tables the "Location of Displacement" is the distance from the end of the cable to the imposed displacement or the accelerometer location.

Table 4.10 Summary of the Number of Cycles to the First Wire Break in Test Specimen 1 through 6

Specimen Number	Number of Strands	Displacement (+/- in.)	Location of Displacement (ft)	First Wire Break
Cable Stay 1 (grouted)*:	19	1.6	16.5	300,000
Cable Stay 2 (grouted)*:	19	1.6	16.5	420,000
Cable Stay 3 (grouted):	19	1.6	16.5	1,100,000
Cable Stay 4 (grouted):	19	1.1	16.5	2,850,000
Cable Stay 5 (ungrouted):	19	1.6	16.5	**

* (Poser 2002)

** No wire breaks occurred in specimen 5 after 5,210,000 Cycles

Table 4.11 Summary of Estimated Fatigue for Seven Fred Hartman Stay Cables

Cable ID	Number of Strands	Equivalent Displacement (in.)	Location of Displacement (ft)	Total Number of Cycles
AS1:	61	9.4	51	31,233
AS5:	43	12.1	52	323,179
AS9:	31	11.5	37	108,827
AS16:	31	11.1	38	93,041
AS23:	55	11.6	65	70,674
AS24:	55	13.4	60	27,057
AN24:	55	7.9	63	20,042

Note that all the test specimens experienced a relatively high number of cycles compared to the bridge cables but the amount of displacement and the location of the displacements are not the same for both the specimens and the bridge cables. It is important to note that all of the cables in Table 4.10 are larger in diameter and have more strands than the 19-strand test specimen. Because of this difference, the stress induced by the same displacement will be higher in the bridge cables for the same displacement. Because the FEM models developed on this project are not able to correlate the displacement of a cable to the stress at the ends, there is no way to compare these results. Future FEM models should be able to estimate the stresses in any size cable based on a given displacement and displacement location. It is anticipated that future researchers will be able to evaluate the fatigue damage based on a refined FEM model and the results presented in this chapter.

4.6 RECOMMENDATION FOR FUTURE RESEARCH

Further research needs to be performed to verify the results of this chapter. The equivalent displacement and cycles/minute are based on a limited number of records and should include more records of wind-rain induced vibration. To do this the process should be automated to improve efficiency. In addition the

analysis should include all of the cables that were instrumented with accelerometers so the results can be more easily applied to all the cables on the bridge.

Another improvement for the analysis would be to analyze each one-minute segment included in the JHU database. While this may be an arduous task, it would lead to a much more accurate estimate of the amount of time each cable has undergone wind-rain induced vibrations. The more accurate estimate should be less than the estimate presented in this chapter and should also provide a better confidence level.

When a refined FEM model is complete, these results should be analyzed. When the stress in the Fred Hartman cables is better understood, the 19-strand tests can be modified to better resemble the stresses in the bridge cables. In addition, the results presented in this chapter can be used to estimate the fatigue damage of each bridge cable due to wind-rain induced vibrations.

CHAPTER 5
Summary and Conclusions

This thesis was prepared to assist the research team with the fatigue analysis of the Fred Hartman Bridge stay cables. While this thesis does not report the results of any full-scale cable tests, it does provide information to assist the research team with future research. The three topics discussed in this thesis include:

1. Static tests of single-strand specimens under tension and bending and the development of the associated closed-form solutions for a simply-supported beam and a fixed-fixed beam. The results of the single-strand test are compared with the 19-strand specimens and the closed-form solutions.
2. Tensile fatigue testing of representative strand used to construct the full-scale specimens 1 through 6. The results are compared with published strand fatigue data and PTI specifications.
3. Characterization of the cable stay vibration data from the Fred Hartman Bridge. The vibration data were used to estimate the fatigue damage to the Fred Hartman cables due to wind-rain induced vibration.

5.1 SINGLE-STRAND BENDING TESTS

The single-strand bending tests provided information about the bending characteristics of single-strand specimens under tension. The results of these tests

and the associated closed-form solutions should assist the research team with improving the FEM models for the 19-strand specimen. Important information obtained with these tests includes:

- The strain due to bending is essentially zero 12 in. from the face of the chuck, which agrees with the closed-form solution, for a fixed-fixed beam.
- Based on the stiffness comparison between the single-strand tests and grouted and ungrouted 19-strand tests, it appears that the grout has only a minor influence on the stiffness of the 19-strand specimens.
- The single-strand specimens were approximately 2% less stiff than the stiffness calculated using the closed form solution for a fixed-fixed beam and approximately 4% more stiff than the stiffness calculated using the closed-form solution for a simply-supported beam. This concludes that the two models are upper and lower bounds to the actual stiffness of the strand.
- The measured response of individual single-strand indicated that the single-strand specimen became slightly stiffer as mid-point deflection increased. The most probable reason for the increase in stiffness is an increase in tension during bending. This phenomenon was not considered in the closed-form solution.
- An effective EI of 0.94EI can be used in the fixed-fixed beam solution to attain the observed response of a single strand.
- Based on the moment comparison between the single-strand tests and the closed-form solutions, it appears that the calculated

moment in the strand is less than the closed form solution for the fixed-fixed beam.

5.2 STRAND TENSION FATIGUE TESTS

The strand tension fatigue tests were used to develop the fatigue characteristics of the strand used to construct Stay Cable Tests 1 through 6. Results of the tests indicate that the fatigue characteristic of the strand do not meet the 1986 or the 2001 PTI specifications. The strand however does fall between the minimum and mean of strand fatigue data published by Paulson (1983). Recommendations for the strand tension fatigue tests include:

- Additional strand fatigue tests should be performed at stress ranges other than 20, 30, and 40 ksi. to develop a complete S-N curve for the strand
- When the stress in the strands of the 19-strand specimens is better defined, strand fatigue tests should be performed at those stress ranges. With the additional information from these tests, the failure mechanism of the wires in the 19-strand specimens and hence the Fred Hartman bridge should be better understood.
- A test should be developed to conduct fatigue tests of grouted single strands. These results will assist in the identification of fretting and the associated reduction in fatigue life due to fretting.

5.3 FRED HARTMAN CABLE VIBRATION CHARACTERIZATION

Acceleration records from cable vibration events on the Fred Hartman Bridge were characterized in terms of the following characteristics:

- The displacement of cable at the accelerometer location
- Primary vibration frequencies and mode of the cable vibration
- The equivalent displacement and the associated cycles/minute for each cable
- The total number of cycles that each cable has undergone since construction of the bridge in September of 1995.

After characterization of the cable stay vibrations the calculated displacement record was used to estimate the equivalent displacement of each bridge cable analyzed. Using the database developed by researchers at Johns Hopkins the total number of cycles that each cable experienced was also estimated. It is not possible to relate these results to fatigue damage because of the differences in calculated displacement location and cable size. However, it was concluded that a refined FEM model needs to be developed to relate the deflection of the cables to stress at the ends. With this refined model, the results presented in Chapter 4 can be used to evaluate the fatigue damage in the Fred Hartman stay-cables.

The following are recommendations for improving this analysis:

- More than ten wind-rain vibrations records should be characterized. If possible, the process should be automated for efficiency. In addition, all the cables that had accelerometers should be included in the analysis.
- The one-minute acceleration records from the database should be analyzed for a better prediction of the total number of cycles that each cable has undergone. This process should also be automated to improve efficiency.

- After the refined FEM model is complete, the stresses in the Fred Hartman cables should be estimated so that the 19-strand tests can be adjusted to simulate the bending stresses seen in the bridge cables. The results of these improved tests should provide better estimates of the actual fatigue damage.

Appendix A
Closed-Form Solutions

The derivation of both closed-form solutions were developed with the following parameters:

- The strand is viewed as a tension strut with a transverse force at mid-span
- To include secondary bending effects due to the tension in the strand, the free-body diagram (FBD) includes an initial deflection due to the transverse load. This is similar to the derivation of a compression member with secondary bending (i.e. Euler buckling), except the solution is stable due to the tension in the strand.
- Deformation due to shear was ignored due to the large span-to-depth ratio of the strand.
- Because the transverse load is located at mid-span, the solutions for both cases are symmetric. Therefore the solutions are derived for only half of the beam.

A.1 Fixed-Fixed Beam with Axial Tension and Bending

Figure A.1 shows the free body diagram used to establish the equilibrium equation for the fixed-fixed beam. The equilibrium equation is developed by summing the moments about an arbitrary point at a distance x, along the beam.

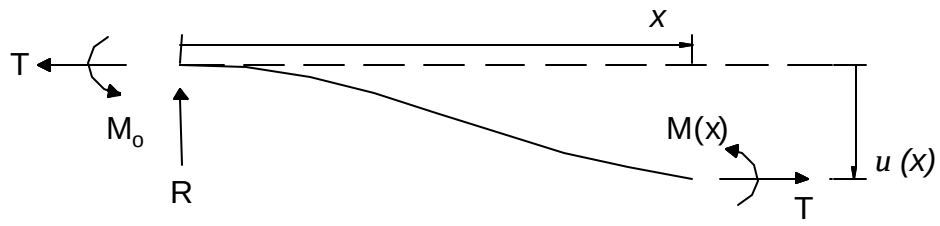

Figure A.1 Fixed-Fixed Beam Free Body Diagram

A.1.1 Derivation

Equilibrium Equation **Substitutions**

$$M(x) = R\cdot x - T\cdot v(x) - M_o$$

$$-E\cdot I\cdot\frac{d^2}{dx^2}v(x) = R\cdot x - T\cdot v(x) - M_o \qquad M(x) = -EI\cdot\frac{d^2}{dx^2}v(x)$$

$$\frac{d^2}{dx^2}v(x) - \frac{T}{E\cdot I}\cdot v(x) = \frac{-P}{2\cdot E\cdot I}\cdot x + \frac{M_o}{E\cdot I} \qquad R = \frac{P}{2}$$

Governing Differential Equation

$$\frac{d^2}{dx^2}v(x) - \lambda^2\cdot v(x) = \frac{-P}{2\cdot E\cdot I}\cdot x + \frac{M_o}{E\cdot I} \qquad \lambda^2 = \frac{T}{E\cdot I}$$

General Solutions

$$v(x) = A\cdot\sinh(\lambda\cdot x) + B\cdot\cosh(\lambda\cdot x) + C\cdot x + D$$

$$\frac{d}{dx}v(x) = A\cdot\lambda\cdot\cosh(\lambda\cdot x) + B\cdot\lambda\cdot\sinh(\lambda\cdot x) + C$$

$$\frac{d^2}{dx^2}v(x) = A\cdot\lambda^2\cdot\sinh(\lambda\cdot x) + B\cdot\lambda^2\cdot\cosh(\lambda\cdot x)$$

Solve for C and D

$$\frac{d^2}{dx^2}v(x) - \lambda^2 \cdot v(x) = -(C \cdot x + D) \cdot \lambda^2$$

$$-C \cdot \lambda^2 - D \cdot \lambda^2 = \frac{-P}{2 \cdot E \cdot I} \cdot x + \frac{M_o}{E \cdot I}$$

$$-C \cdot \lambda^2 = \frac{-P}{2 \cdot E \cdot I} \cdot x \qquad -D \cdot \lambda^2 = \frac{M_o}{E \cdot I}$$

$$C = \frac{P}{2T} \qquad D = \frac{-M_o}{T}$$

Use Boundry Conditions to Solve for A and B

$$v(0) = 0$$

$$B = \frac{M_o}{T}$$

$$\frac{d}{dx}v(0) = 0$$

$$A = \frac{-P}{2T \cdot \lambda}$$

Particular Solutions for Fixed-Fixed Beam

$$v(x) = \frac{-P}{2T \cdot \lambda} \cdot \sinh(\lambda \cdot x) + \frac{M_o}{T} \cdot \cosh(\lambda \cdot x) + \frac{P}{2T} \cdot x - \frac{M_o}{T}$$

$$\frac{d}{dx}v(x) = \frac{-P}{2 \cdot T} \cdot \cosh(\lambda \cdot x) + \frac{M_o}{T} \cdot \lambda \cdot \sinh(\lambda \cdot x) + \frac{P}{2 \cdot T}$$

$$\frac{d^2}{dx^2}v(x) = \frac{-P}{2 \cdot T} \cdot \lambda \cdot \sinh(\lambda \cdot x) + \frac{M_o}{T} \cdot \lambda^2 \cdot \cosh(\lambda \cdot x)$$

Solve for Mo

since load is at mid-span,

$$M_O = M\left(\frac{L}{2}\right) \quad \text{and,}$$

$$\frac{d}{dx}v\left(\frac{L}{2}\right) = 0$$

$$M_O = \frac{P \cdot L}{2} \cdot \left[\frac{\left(\cosh\left(\frac{L}{2}\cdot\lambda\right) - 1\right)}{\sinh\left(\frac{L}{2}\cdot\lambda\right)}\right]$$

A.1.2 Fixed-Fixed Beam Deflected Shape

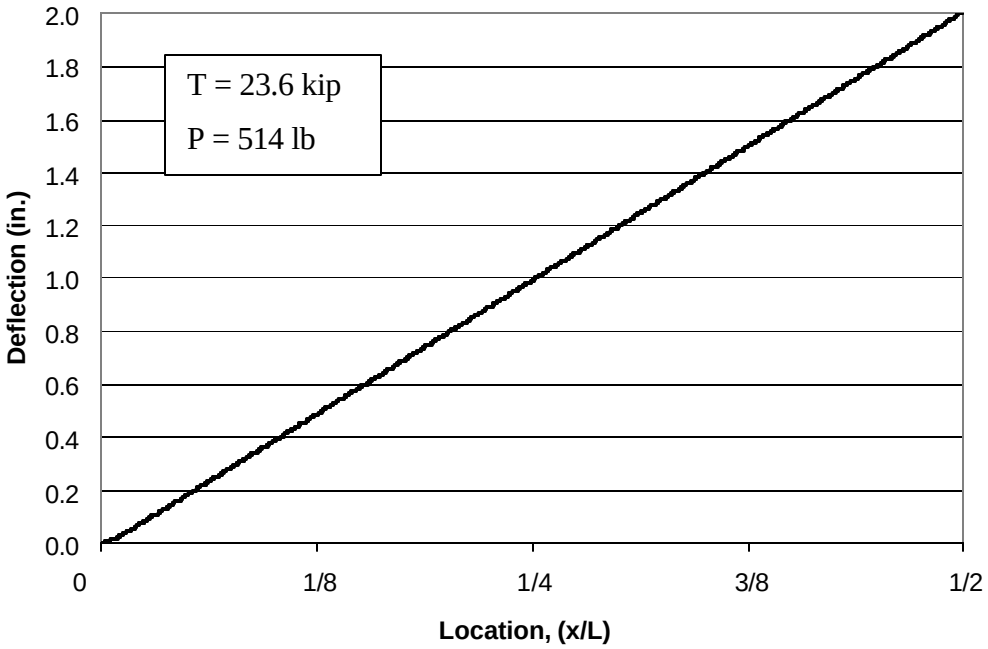

Figure A.2 Fixed-Fixed Beam Deflection Diagram

A.1.3 Moment Diagram

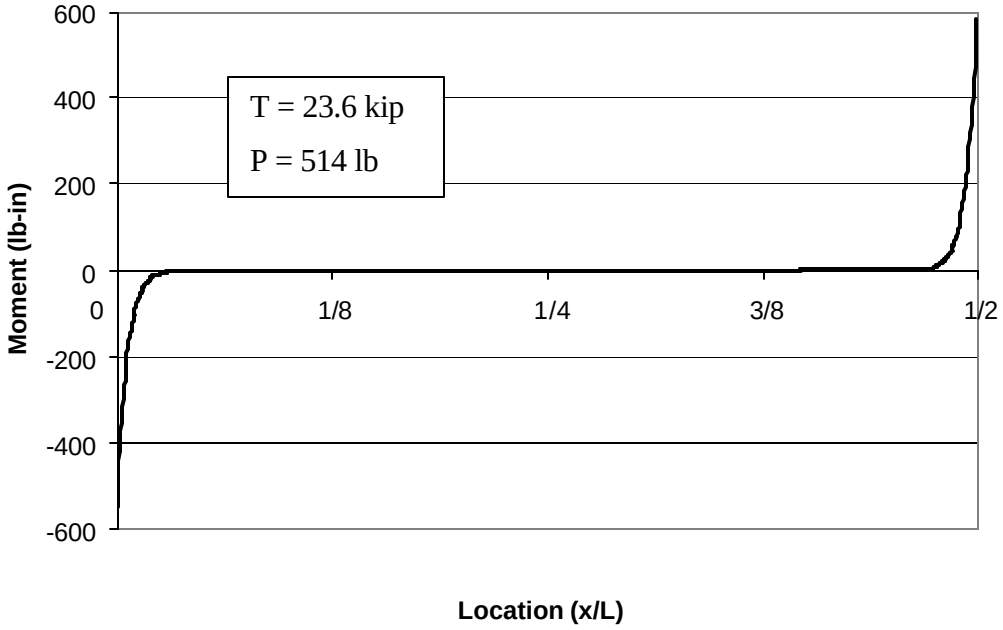

Figure A.3 Fixed-Fixed Beam Moment Diagram

To verify the validity of the fixed-fixed beam solution, the moment was plotted for a very small tension (Fig. A.4). As T goes to zero in the fixed-fixed beam solution, the moment at the ends and at the mid-point should go to PL/8. For Figure A.4, the transverse load is 514 lb, T is $1x10^{-7}$ kip, and all other parameters are the same as the strand. For this case PL/8 = 25,443 lb-in. which equals the maximum moment in Figure A.4. The moment for the fixed-fixed beam solution is much higher when the tension in the strand is close to zero because with no tension in the strand, there is a significant increase in curvature at the ends and mid-span. As expected, as T increases the beam acts less like a pure beam due to the secondary effects from the tension.

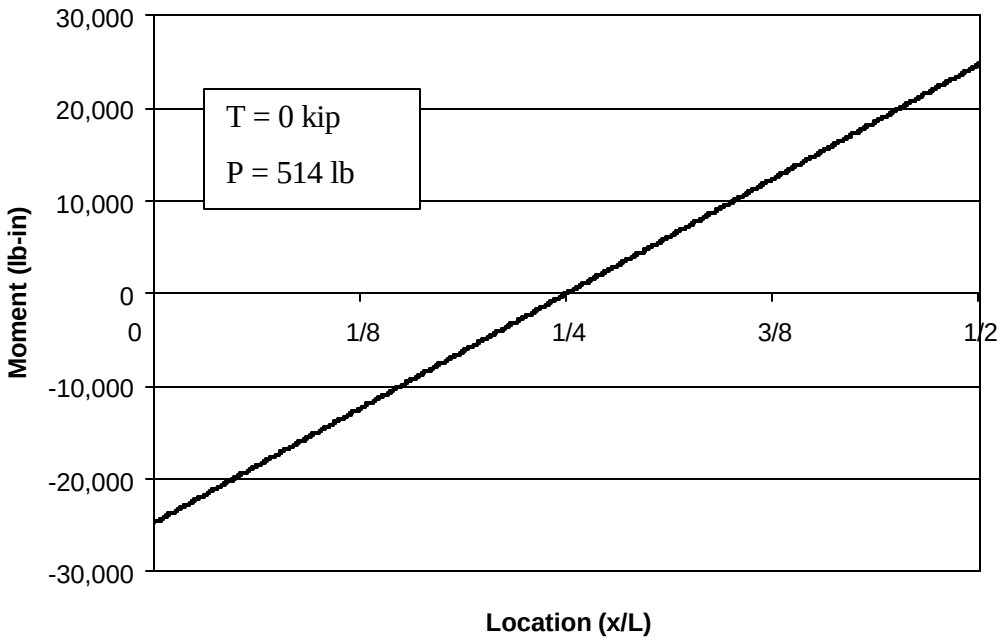

Figure A.4 Fixed-Fixed Beam Moment Diagram for T ˜ 0 kip

A.2 SIMPLY SUPPORTED BEAM WITH AXIAL TENSION AND BENDING

Figure A.4 shows the free body diagram used to develop the equilibrium equation for the simply-supported solution. The primary difference between the fixed-fixed solution and the simply-supported solution is the reaction moment at the beam ends. The deflection diagram (Fig. A.4) and the moment diagram (Fig. A.6) are associated with a transverse load of 482 lb which results in a stiffness of 241 lb/in.

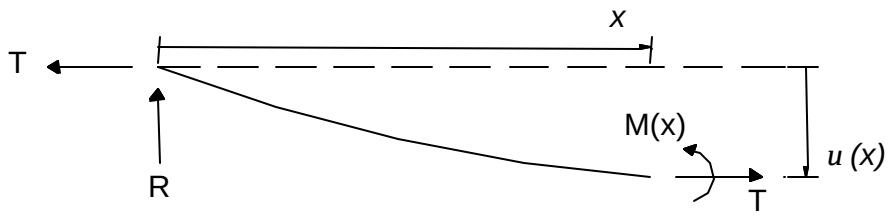

Figure A.5 Simply-Supported Beam Free Body Diagram

A.2.1 Derivation

Equilibrium Equation **Substitutions**

$$M(x) = R\cdot x - T\cdot v(x)$$

$$-E\cdot I\cdot\frac{d^2}{dx^2}v(x) = R\cdot x - T\cdot v(x) \qquad M(x) = -EI\cdot\frac{d^2}{dx^2}v(x)$$

$$\frac{d^2}{dx^2}v(x) - \frac{T}{E\cdot I}\cdot v(x) = \frac{-P}{2\cdot E\cdot I}\cdot x \qquad R = \frac{P}{2}$$

Governing Differential Equation

$$\frac{d^2}{dx^2}v(x) - \lambda^2\cdot v(x) = \frac{-P}{2\cdot E\cdot I}\cdot x \qquad \lambda^2 = \frac{T}{E\cdot I}$$

General Solutions

$$v(x) = A\cdot\sinh(\lambda\cdot x) + B\cdot\cosh(\lambda\cdot x) + C\cdot x$$

$$\frac{d}{dx}v(x) = A\cdot\lambda\cdot\cosh(\lambda\cdot x) + B\cdot\lambda\cdot\sinh(\lambda\cdot x) + C$$

$$\frac{d^2}{dx^2}v(x) = A\cdot\lambda^2\cdot\sinh(\lambda\cdot x) + B\cdot\lambda^2\cdot\cosh(\lambda\cdot x)$$

Solve for C

$$\frac{d^2}{dx^2}v(x) - \lambda^2 \cdot v(x) = -C \cdot x \cdot \lambda^2$$

$$-C \cdot \lambda^2 = \frac{-P}{2 \cdot E \cdot I} \cdot x$$

$$-C \cdot \lambda^2 = \frac{-P}{2 \cdot E \cdot I} \cdot x$$

$$C = \frac{P}{2T}$$

Use Boundry Conditions to Solve for A and B

$$v(0) = 0$$

$$B = 0$$

$$\frac{d}{dx}v\left(\frac{L}{2}\right) = 0$$

$$A = \frac{-P}{2T \cdot \lambda \cdot \cosh\left(\lambda \cdot \frac{L}{2}\right)}$$

Particular Solutions for Simply-Supported Bea

$$v(x) = \frac{-P}{2 \cdot T \cdot \lambda} \cdot \frac{\sinh(\lambda \cdot x)}{\cosh\left(\lambda \cdot \frac{L}{2}\right)} + \frac{P}{2 \cdot T} \cdot x$$

$$\frac{d}{dx}v(x) = \frac{-P}{2 \cdot T} \cdot \frac{\cosh(\lambda \cdot x)}{\cosh\left(\lambda \cdot \frac{L}{2}\right)} + \frac{P}{2 \cdot T}$$

$$\frac{d^2}{dx^2}v(x) = \frac{-P}{2 \cdot T} \cdot \lambda \cdot \frac{\sinh(\lambda \cdot x)}{\cosh\left(\lambda \cdot \frac{L}{2}\right)}$$

A.2.2 Simply-Supported Beam Defected Shape

Figure A.6 shows the deflected shape for a simply-supported beam with a tension of 23.6 kip and a transverse load at the midpoint of 482 lb. This correlates to a maximum deflection of 2.0 in.

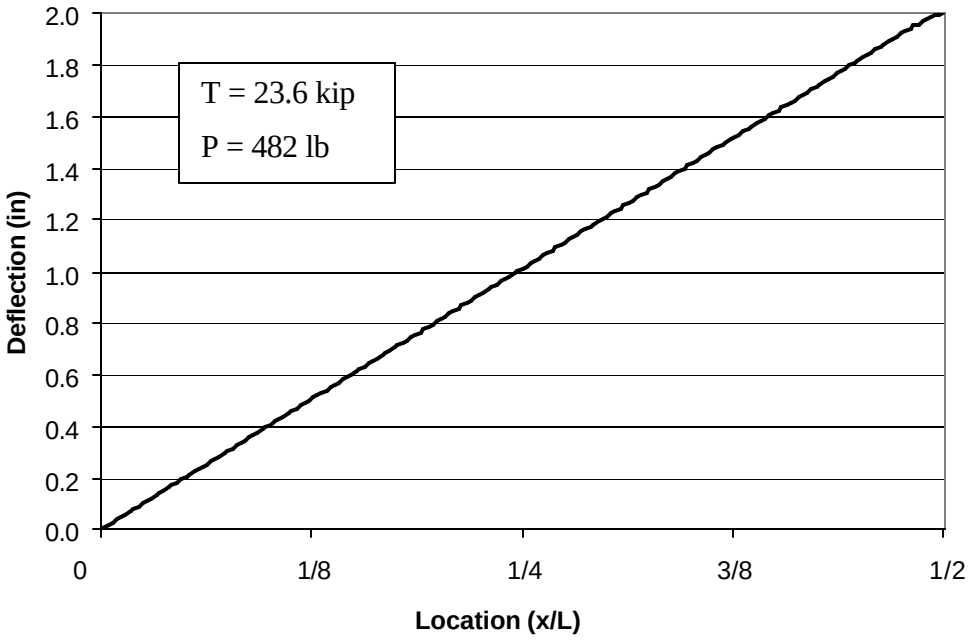

Figure A.6 Simply-Supported Deflected Shape

A.2.3 Moment Diagram

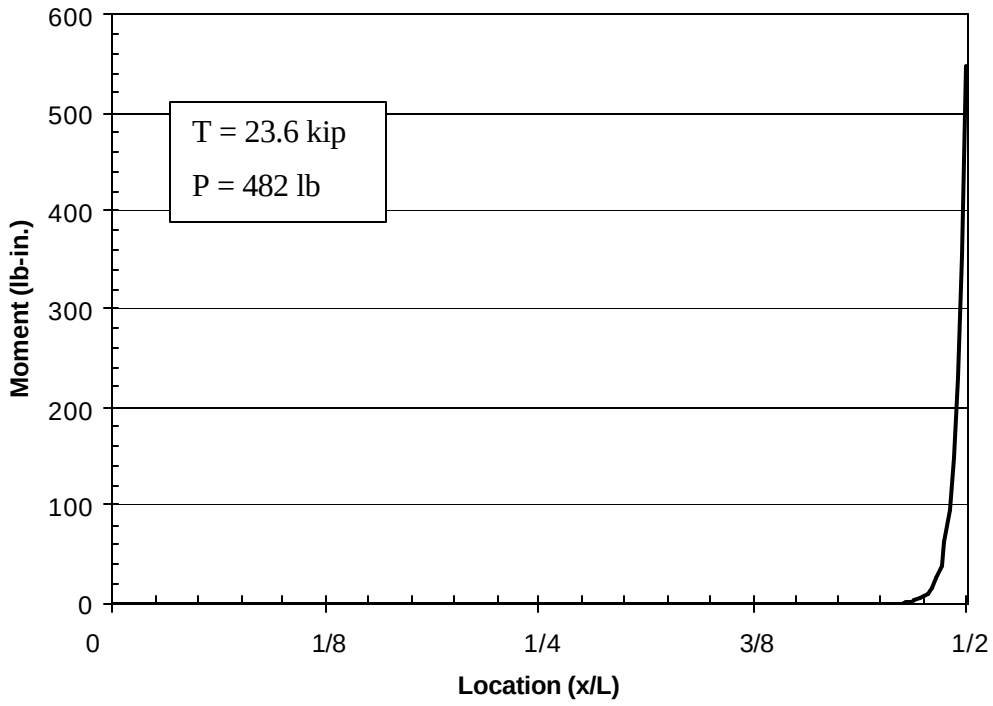

Figure A.7 Simply-Supported Beam Moment Diagram

To verify the validity of the simply-supported beam solution, the moment was plotted for a very small tension (Fig. A.8). As T goes to zero in the simply-supported beam solution, the moment at the mid-point should go to PL/4. For Figure A.4, the transverse load is 482 lb, T is $1x10^{-7}$ kip, and all other parameters are the same as the strand. For this case PL/4 = 47,713 lb-in. which equals the maximum moment in Figure A.8. Similar to the fixed-fixed solution, when T is close to zero the moment in the strand is significantly increased due to the increase in curvature at mid-span. As expected, as T increases the beam acts less like a pure beam due to the secondary effects from the tension.

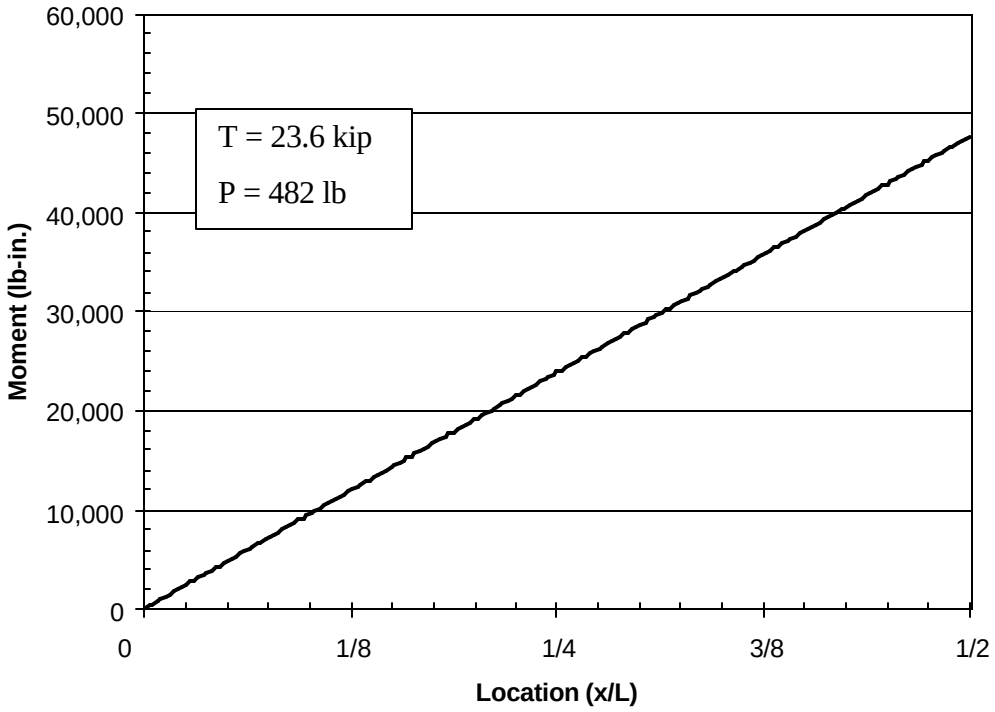

Figure A.8 Simply-supported Beam Moment Diagram for T ~ 0 kip

Appendix B
Single-Strand Bending Tests

The single-strand bending tests were performed with three different strand specimens. For each specimen two or three tests were performed at different prestress levels. Note that each test was repeated at least twice. Only one cycle of each test is included in this appendix because the responses of the tests were within 5 % of each other for each cycle. Also note that tests performed at low prestress levels (less than 4 kip) are not included in this appendix because the variation in strain was extremely small.

Strains measured by all functioning gages are plotted against mid-span deflection of the strand in this appendix. Note that at least one of the strain gages failed to yield useful data due to damage or de-bonding from the strand in all the tests. Data from these gages are not plotted. The strand specimen number and the test number are indicated in the title of each plot and the gage location is indicated within each plot. Table B.1 provides a summary of the tests and indicates which strain gage data was plotted for each test.

Also included in this appendix is a copy of the manufacturer's specification sheet for the strand used in the single-strand bending tests, the strand tension fatigue tests, and the full-sized stay-cable bending fatigue tests (Fig. B.17).

In addition, this appendix includes data collected for verification of the size of the strand. For a strand sample, the area of each wire was measured and tabulated (Fig. B.18).

Table B.1 Single Strand Test Summary

		Prestress	Strain Gages										
Strand	**Test**	**(kip)**	**A1**	**A2**	**A3**	**A4**	**A5**	**A6**	**B1**	**B2**	**B3**	**B4**	**B5**	**B6**
1	1	7.5	X		X		X	X	X	X	X			
1	2	21.4	X		X		X	X	X	X	X			
2	1	14.5	X	X	X		X	X	X	X	X			
2	2	20.9	X	X	X		X	X	X	X	X			
2	3	23.3	X	X	X		X	X	X	X	X			
3	1	21.9	X	X	X		X	X	X	X	X	X	X	
3	2	23.5	X	X	X		X	X	X	X	X	X	X	
3	3	30.9	X	X	X		X	X	X	X	X	X	X	

X indicates a strain gage that worked throughout the test. These strain gages are plotted.

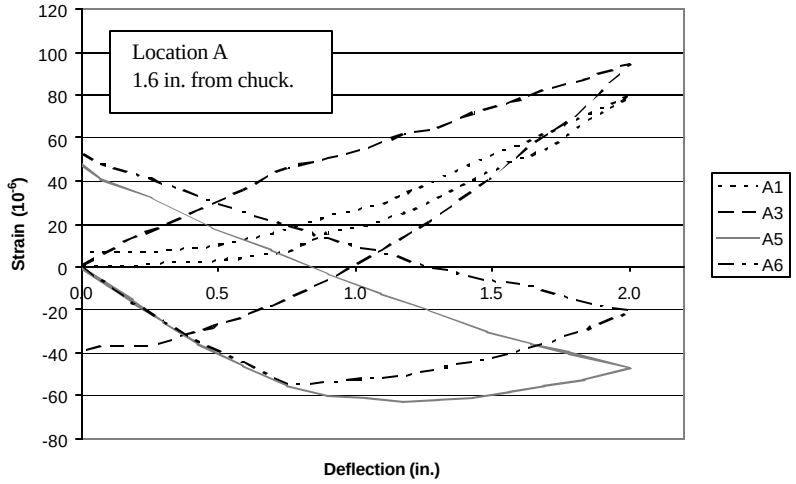

Figure B.1 Strand 1, Test 1 at a Prestress of 7.5 kip

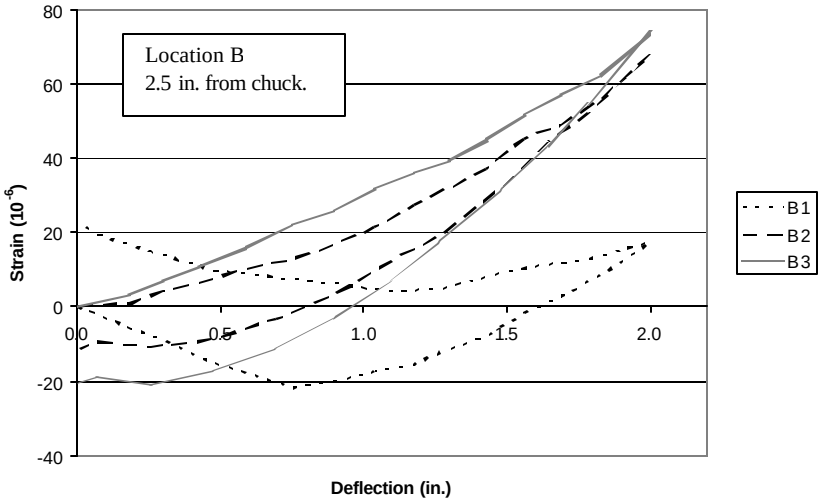

Figure B.2 Strand 1, Test 1 at a Prestress of 7.5 kip

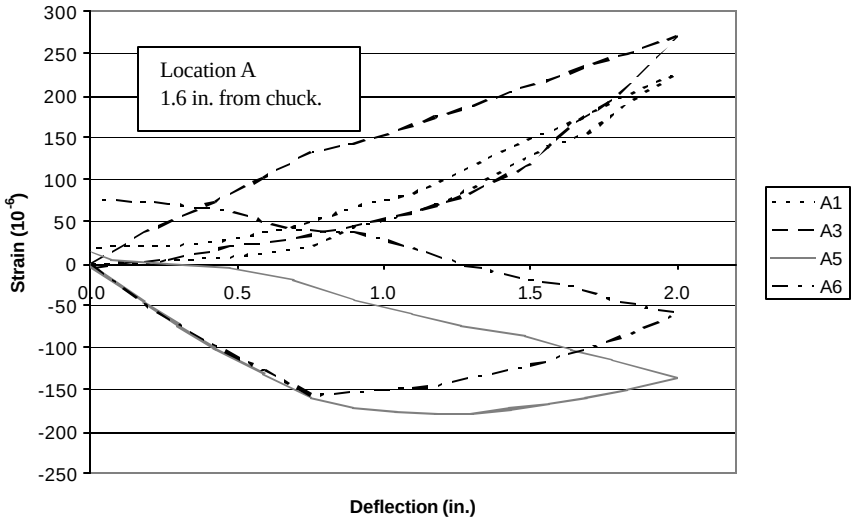

Figure B.3 Strand 1, Test 2 at a Prestress of 21.4 kip

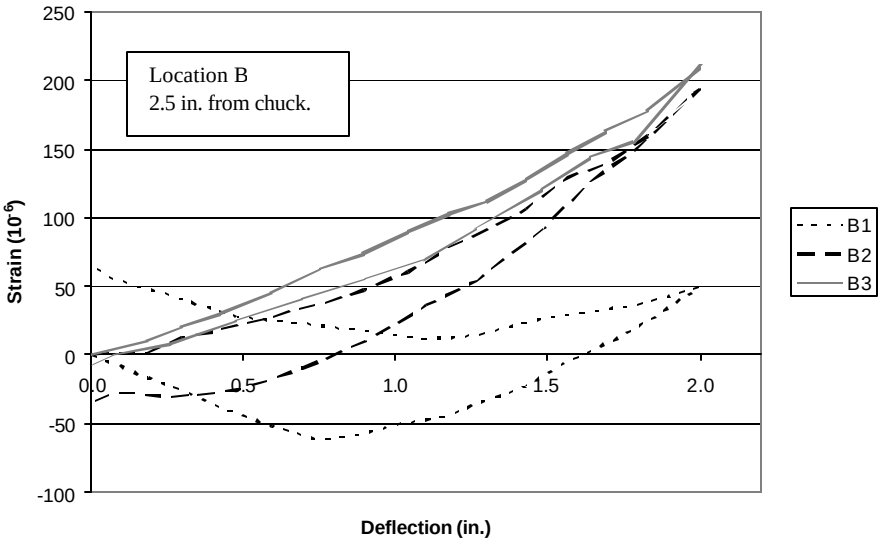

Figure B.4 Strand 1, Test 2 at a Prestress of 21.4 kip

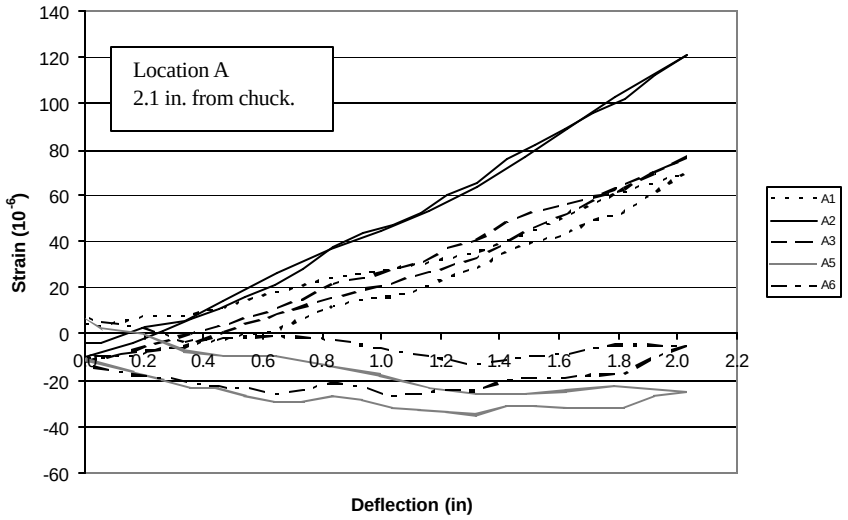

Figure B.5 Strand 2, Test 1 at a Prestress of 14.5 kip

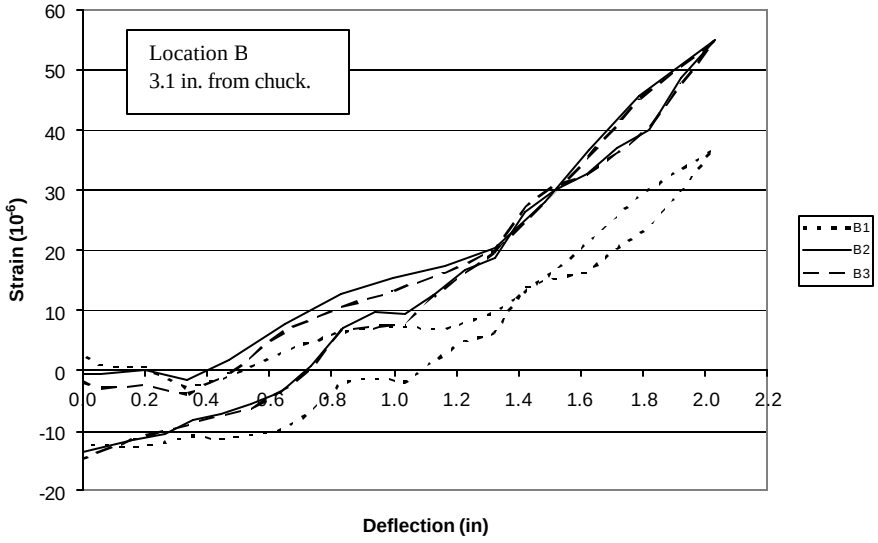

Figure B.6 Strand 2, Test 1 at a Prestress of 14.5 kip

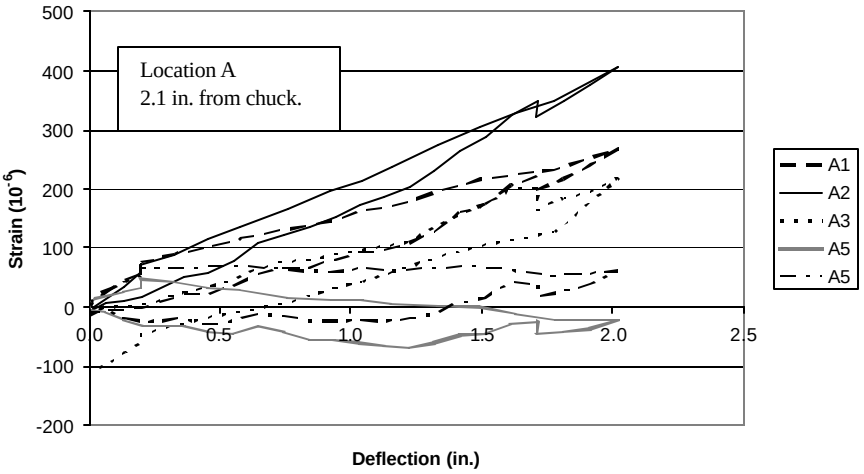

Figure B.7 Strand 2, Test 2 at a Prestress of 20.9 kip

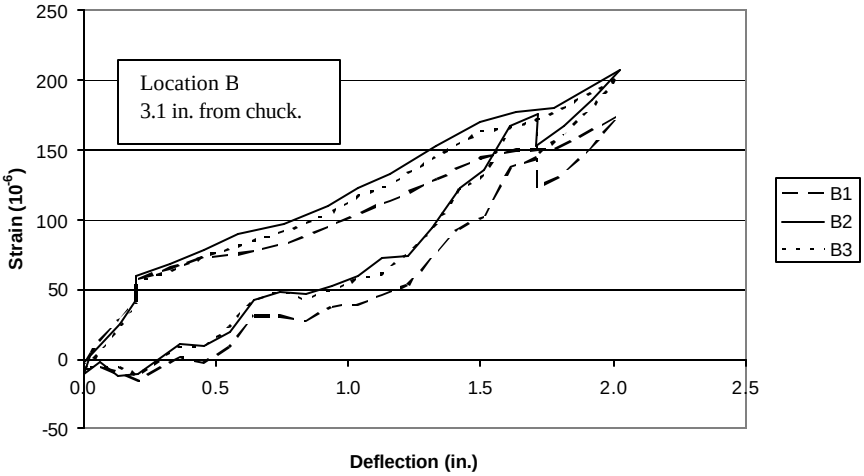

Figure B.8 Strand 2, Test 2 at a Prestress of 20.9 kip

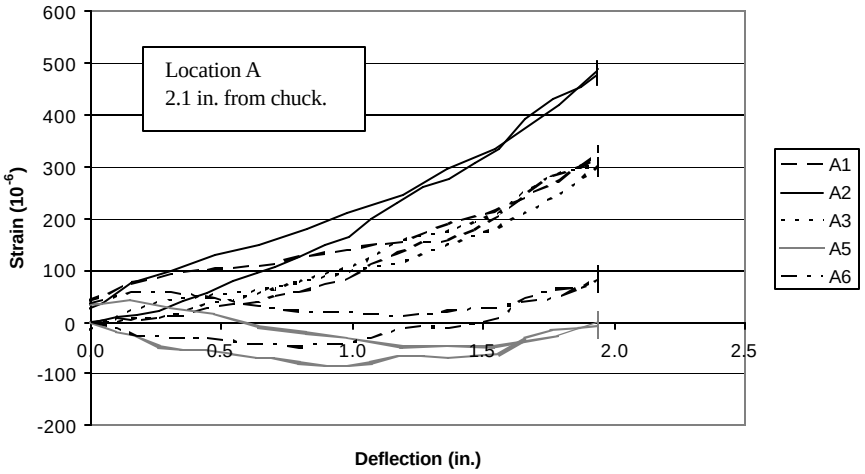

Figure B.9 Strand 2, Test 3at a Prestress of 23.3 kip

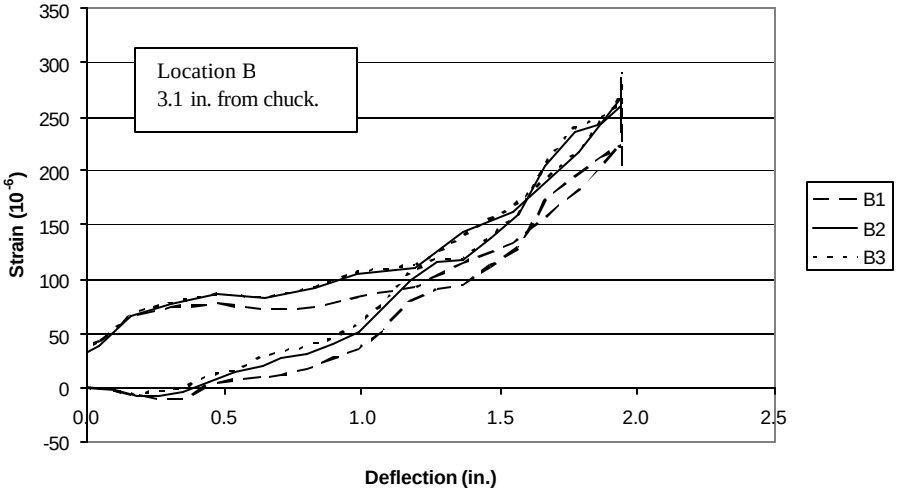

Figure B.10 Strand 2, Test 3 at a Prestress of 23.3 kip

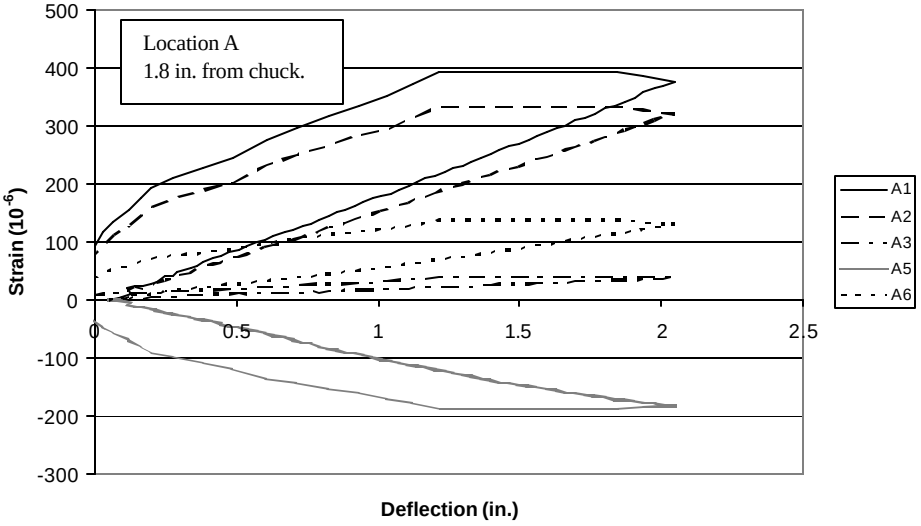

Figure B.11 Strand 3, Test 1 at a Prestress of 21.9 kip

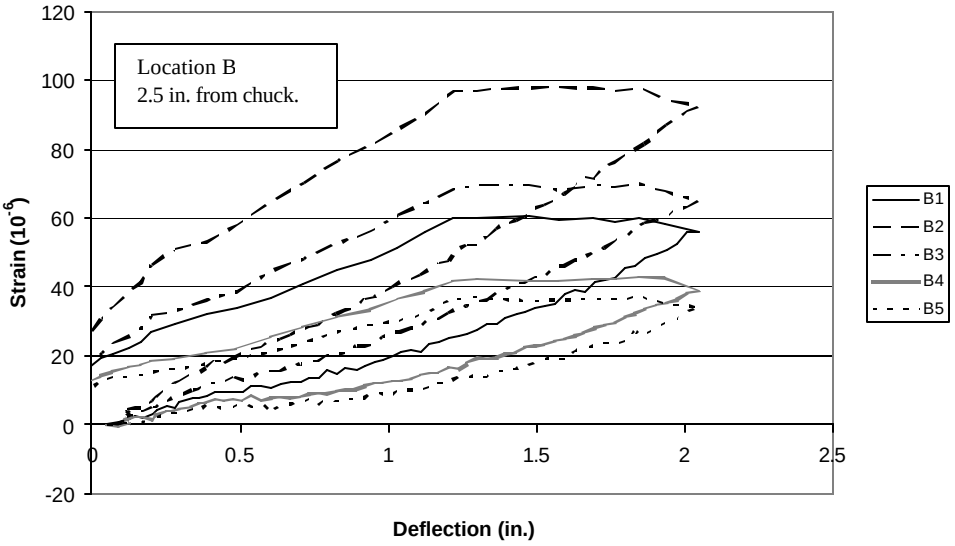

Figure B.12 Strand 3, Test 1 at a Prestress of 21.9 kip

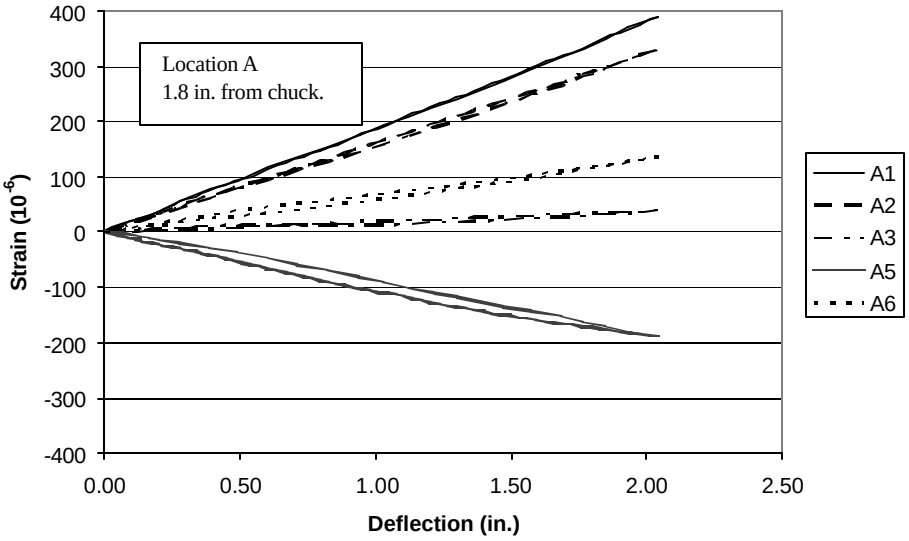

Figure B.13 Strand 3, Test 2 at a Prestress of 23.5 kip

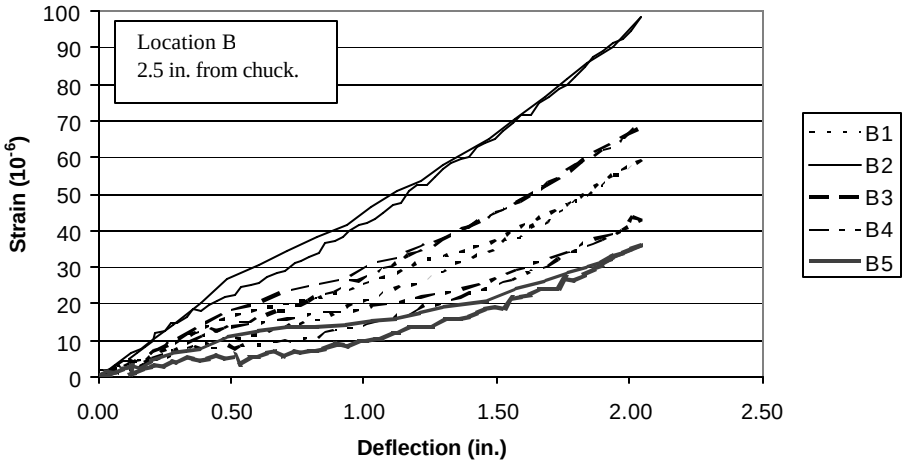

Figure B.14 Strand 3, Test 2 at a Prestress of 23.5 kip

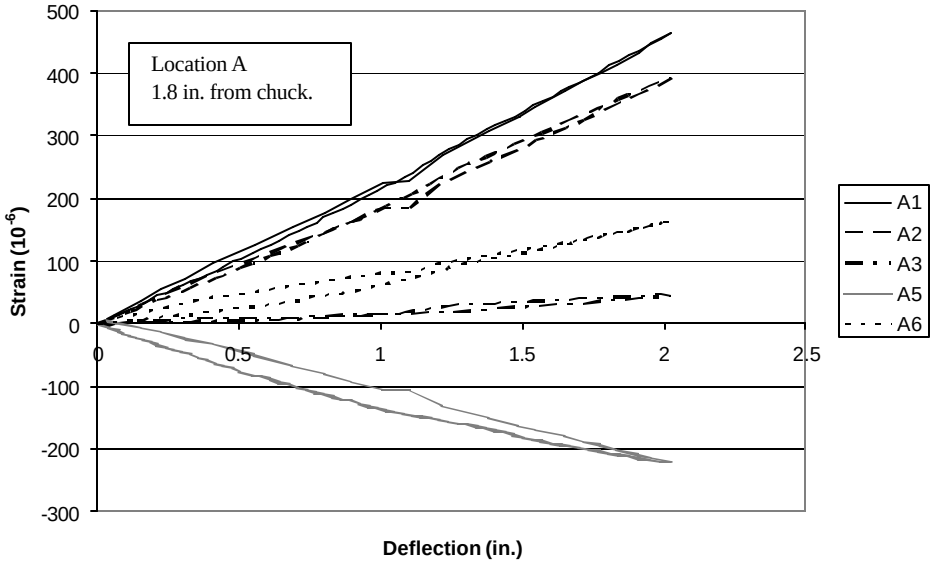

Figure B.15 Strand 3, Test 3 at a Prestress of 30.8 kip

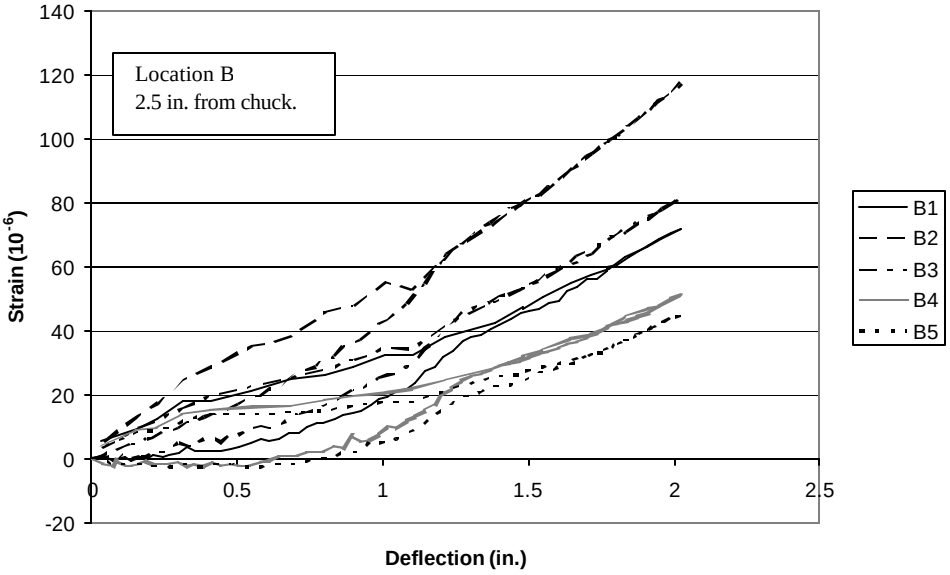

Figure B.16 Strand 3, Test 3 at a Prestress of 30.8 kip

Figure B.17 Strand Specification Sheet

A sample strand was used to measure the area of each wire to verify the size of the strand used in the single strand tests and the full-scale specimens 1 through 6. The measure the area of each wire, the sample strand was unwound into 7 separate wires. Each wire was measured to be 6 $^{1}/_{16}$-in. long. Each wire was placed in a graduated cylinder filled with water. The displacement of each wire was recorded and the area of each wire was ten calculated (Fig. B.18). The total measured area of the strand was essentially the same as the area provided by the manufacturer (Fig. B.17).

Wire No.	Wire Location	Length (in)	Volume (mL)	Volume (in^3)	Area (in^2)
1	outer	6.1875	3.13	0.191	0.031
2	outer	6.1875	3.12	0.190	0.031
3	outer	6.1875	3.13	0.191	0.031
4	outer	6.1875	3.12	0.190	0.031
5	outer	6.1875	3.14	0.192	0.031
6	outer	6.1875	3.13	0.191	0.031
7	inner	6.1875	3.30	0.201	0.033
				Total Area (in^2):	**0.218**

Figure B.18 Strand Size Verification

Appendix C
Rainflow Analysis Results

The rainflow analysis results from CRUNCH (Buhl 2002) are presented in this appendix. For each wind-rain vibration file there are two rainflow results tables provided. The first is the raw output from CRUNCH and the second is the modified rainflow counts excluding all cycles with a displacement range of less than 3 in. For a thorough explanation of the CRUNCH rainflow algorithm see Buhl (2002).

In each table, the amplitude range of each bin is 1 in. except the first bin which has an amplitude range of ½ in. The cycle counts for each cable are provided in units of cycles per time. Because each displacement record is 5 minutes, the number of cycles occurring in 5 minutes is tabulated. The file numbers associated with each table correlate to the date the file was recorded. The first 8 numbers represent the year, month, and day respectively that the file was recorded. The last one or two digits corresponds to the number of the recording on that date. For example file number 1997100111 is the 11^{th} file recorded on October 1, 1997. The "D_" prefix on each file name indicates that the file was a displacement history.

Rainflow counts for file D_199710111

Bins (in)	AS1 (cyc/time)	AS5 (cyc/time)	AS9 (cyc/time)	AS16 (cyc/time)	AS23 (cyc/time)	AS24 (cyc/time)	AN24 (cyc/time)
0.5	926	1151	691	60	184	26	422
1.5	0	0	220	0	1	0	137
2.5	0	0	1	1	45	0	242
3.5	0	0	0	42	58	0	93
4.5	0	0	0	148	40	13	18
5.5	0	0	0	196	21	77	1
6.5	0	0	0	108	21	21	0
7.5	0	0	0	53	15	13	0
8.5	0	0	0	14	13	14	0
9.5	0	0	0	16	36	12	0
10.5	0	0	0	29	83	11	0
11.5	0	0	0	14	77	10	0
12.5	0	0	0	30	51	7	0
13.5	0	0	0	17	38	13	0
14.5	0	0	0	17	7	7	0
15.5	0	0	0	29	1	15	0
16.5	0	0	0	27	0	31	0
17.5	0	0	0	4	0	49	0
18.5	0	0	0	0	0	98	0
19.5	0	0	0	0	0	180	0
S(cyc/time) :	926	1151	912	805	691	597	913

Appendix D

Rainflow counts for file D_199710111 excluding bins less than 3 in.

Bins (in)	AS1 (cyc/time)	AS5 (cyc/time)	AS9 (cyc/time)	AS16 (cyc/time)	AS23 (cyc/time)	AS24 (cyc/time)	AN24 (cyc/time)
0.5	0	0	0	0	0	0	0
1.5	0	0	0	0	0	0	0
2.5	0	0	0	0	0	0	0
3.5	0	0	0	42	58	0	93
4.5	0	0	0	148	40	13	18
5.5	0	0	0	196	21	77	1
6.5	0	0	0	108	21	21	0
7.5	0	0	0	53	15	13	0
8.5	0	0	0	14	13	14	0
9.5	0	0	0	16	36	12	0
10.5	0	0	0	29	83	11	0
11.5	0	0	0	14	77	10	0
12.5	0	0	0	30	51	7	0
13.5	0	0	0	17	38	13	0
14.5	0	0	0	17	7	7	0
15.5	0	0	0	29	1	15	0
16.5	0	0	0	27	0	31	0
17.5	0	0	0	4	0	49	0
18.5	0	0	0	0	0	98	0
19.5	0	0	0	0	0	180	0
S(cyc/time) :	0	0	0	744	461	571	112

Rainflow counts for file D_199807038

Bins (in)	AS1 (cyc/time)	AS5 (cyc/time)	AS9 (cyc/time)	AS16 (cyc/time)	AS23 (cyc/time)	AS24 (cyc/time)	AN24 (cyc/time)
0.5	986	605	38	0	69	474	493
1.5	0	0	0	0	89	30	30
2.5	0	0	0	0	46	36	8
3.5	0	0	0	1	21	31	3
4.5	0	0	0	0	22	16	1
5.5	0	0	0	170	35	38	3
6.5	0	0	0	231	41	78	1
7.5	0	0	0	187	45	52	0
8.5	0	0	0	91	72	6	1
9.5	0	0	0	61	97	0	2
10.5	0	0	0	2	87	0	2
11.5	0	0	0	0	44	0	1
12.5	0	0	0	0	9	0	1
13.5	0	0	0	0	0	0	0
14.5	0	0	0	0	0	0	0
15.5	0	0	0	0	0	0	1
16.5	0	0	0	0	0	0	0
17.5	0	0	0	0	0	0	1
18.5	0	0	0	0	0	0	0
19.5	0	0	0	0	0	0	4
S(cyc/time) :	986	605	38	743	677	761	552

Rainflow counts for file D_199807038 excluding bins less than 3 in.

Bins (in)	AS1 (cyc/time)	AS5 (cyc/time)	AS9 (cyc/time)	AS16 (cyc/time)	AS23 (cyc/time)	AS24 (cyc/time)	AN24 (cyc/time)
0.5	0	0	0	0	0	0	0
1.5	0	0	0	0	0	0	0
2.5	0	0	0	0	0	0	0
3.5	0	0	0	1	21	31	3
4.5	0	0	0	0	22	16	1
5.5	0	0	0	170	35	38	3
6.5	0	0	0	231	41	78	1
7.5	0	0	0	187	45	52	0
8.5	0	0	0	91	72	6	1
9.5	0	0	0	61	97	0	2
10.5	0	0	0	2	87	0	2
11.5	0	0	0	0	44	0	1
12.5	0	0	0	0	9	0	1
13.5	0	0	0	0	0	0	0
14.5	0	0	0	0	0	0	0
15.5	0	0	0	0	0	0	1
16.5	0	0	0	0	0	0	0
17.5	0	0	0	0	0	0	1
18.5	0	0	0	0	0	0	0
19.5	0	0	0	0	0	0	4
S(cyc/time) :	0	0	0	743	473	221	21

Rainflow counts for file D_199711288

Bins (in)	AS1 (cyc/time)	AS5 (cyc/time)	AS9 (cyc/time)	AS16 (cyc/time)	AS23 (cyc/time)	AS24 (cyc/time)	AN24 (cyc/time)
0.5	1042	1068	1227	48	888	941	873
1.5	0	55	3	78	28	58	0
2.5	0	0	0	94	0	43	0
3.5	0	0	0	49	0	23	0
4.5	0	0	0	19	0	14	0
5.5	0	0	0	19	0	4	0
6.5	0	0	0	34	0	0	0
7.5	0	0	0	79	0	0	0
8.5	0	0	0	47	0	0	0
9.5	0	0	0	55	0	0	0
10.5	0	0	0	40	0	0	0
11.5	0	0	0	22	0	0	0
12.5	0	0	0	9	0	0	0
13.5	0	0	0	8	0	0	0
14.5	0	0	0	48	0	0	0
15.5	0	0	0	63	0	0	0
16.5	0	0	0	49	0	0	0
17.5	0	0	0	21	0	0	0
18.5	0	0	0	2	0	0	0
19.5							
S**(cyc/time) :**	1042	1123	1230	784	916	1083	873

Rainflow counts for file D_199711288 excluding bins less than 3 in.

Bins (in)	AS1 (cyc/time)	AS5 (cyc/time)	AS9 (cyc/time)	AS16 (cyc/time)	AS23 (cyc/time)	AS24 (cyc/time)	AN24 (cyc/time)
0.5	0	0	0	0	0	0	0
1.5	0	0	0	0	0	0	0
2.5	0	0	0	0	0	0	0
3.5	0	0	0	49	0	23	0
4.5	0	0	0	19	0	14	0
5.5	0	0	0	19	0	4	0
6.5	0	0	0	34	0	0	0
7.5	0	0	0	79	0	0	0
8.5	0	0	0	47	0	0	0
9.5	0	0	0	55	0	0	0
10.5	0	0	0	40	0	0	0
11.5	0	0	0	22	0	0	0
12.5	0	0	0	9	0	0	0
13.5	0	0	0	8	0	0	0
14.5	0	0	0	48	0	0	0
15.5	0	0	0	63	0	0	0
16.5	0	0	0	49	0	0	0
17.5	0	0	0	21	0	0	0
18.5	0	0	0	2	0	0	0
19.5	0	0	0	0	0	0	0
S**(cyc/time) :**	0	0	0	564	0	41	0

Rainflow counts for file D_1997100628

Bins (in)	AS1 (cyc/time)	AS5 (cyc/time)	AS9 (cyc/time)	AS16 (cyc/time)	AS23 (cyc/time)	AS24 (cyc/time)	AN24 (cyc/time)
0.5	1390	1128	1249	209	356	10	557
1.5	0	0	0	146	58	1	0
2.5	0	0	0	135	165	17	0
3.5	0	0	0	175	125	44	0
4.5	0	0	0	70	45	43	0
5.5	0	0	0	5	99	72	0
6.5	0	0	0	0	13	99	0
7.5	0	0	0	0	0	133	0
8.5	0	0	0	0	0	121	0
9.5	0	0	0	0	0	39	0
10.5	0	0	0	0	0	0	0
11.5	0	0	0	0	0	0	0
12.5	0	0	0	0	0	0	0
13.5	0	0	0	0	0	0	0
14.5	0	0	0	0	0	0	0
15.5	0	0	0	0	0	0	0
16.5	0	0	0	0	0	0	0
17.5	0	0	0	0	0	0	0
18.5	0	0	0	0	0	0	0
19.5	0	0	0	0	0	0	0
S**(cyc/time) :**	1390	1128	1249	740	861	579	557

Rainflow counts for file D_1997100628 excluding bins less than 3 in.

Bins (in)	AS1 (cyc/time)	AS5 (cyc/time)	AS9 (cyc/time)	AS16 (cyc/time)	AS23 (cyc/time)	AS24 (cyc/time)	AN24 (cyc/time)
0.5	0	0	0	0	0	0	0
1.5	0	0	0	0	0	0	0
2.5	0	0	0	0	0	0	0
3.5	0	0	0	175	125	44	0
4.5	0	0	0	70	45	43	0
5.5	0	0	0	5	99	72	0
6.5	0	0	0	0	13	99	0
7.5	0	0	0	0	0	133	0
8.5	0	0	0	0	0	121	0
9.5	0	0	0	0	0	39	0
10.5	0	0	0	0	0	0	0
11.5	0	0	0	0	0	0	0
12.5	0	0	0	0	0	0	0
13.5	0	0	0	0	0	0	0
14.5	0	0	0	0	0	0	0
15.5	0	0	0	0	0	0	0
16.5	0	0	0	0	0	0	0
17.5	0	0	0	0	0	0	0
18.5	0	0	0	0	0	0	0
19.5	0	0	0	0	0	0	0
S**(cyc/time) :**	0	0	0	250	282	551	0

Rainflow counts for file D_1997100710

Bins (in)	AS1 (cyc/time)	AS5 (cyc/time)	AS9 (cyc/time)	AS16 (cyc/time)	AS23 (cyc/time)	AS24 (cyc/time)	AN24 (cyc/time)
0.5	425	3	1	1310	723	1059	468
1.5	45	0	0	41	200	46	61
2.5	35	0	0	0	118	0	79
3.5	27	1	0	0	47	0	68
4.5	25	3	0	0	9	0	52
5.5	27	3	0	0	0	0	58
6.5	24	10	0	0	0	0	46
7.5	28	13	0	0	0	0	21
8.5	24	21	12	0	0	0	10
9.5	52	28	81	0	0	0	22
10.5	46	39	135	0	0	0	29
11.5	47	51	164	0	0	0	30
12.5	38	44	153	0	0	0	22
13.5	24	55	95	0	0	0	19
14.5	26	69	71	0	0	0	2
15.5	20	94	33	0	0	0	0
16.5	5	86	2	0	0	0	1
17.5	1	85	0	0	0	0	0
18.5	1	66	0	0	0	0	0
19.5	0	47	0	0	0	0	0
S(cyc/time) :	920	718	747	1351	1097	1105	988

Rainflow counts for file D_1997100710 excluding bins less than 3 in.

Bins (in)	AS1 (cyc/time)	AS5 (cyc/time)	AS9 (cyc/time)	AS16 (cyc/time)	AS23 (cyc/time)	AS24 (cyc/time)	AN24 (cyc/time)
0.5	0	0	0	0	0	0	0
1.5	0	0	0	0	0	0	0
2.5	0	0	0	0	0	0	0
3.5	27	1	0	0	47	0	68
4.5	25	3	0	0	9	0	52
5.5	27	3	0	0	0	0	58
6.5	24	10	0	0	0	0	46
7.5	28	13	0	0	0	0	21
8.5	24	21	12	0	0	0	10
9.5	52	28	81	0	0	0	22
10.5	46	39	135	0	0	0	29
11.5	47	51	164	0	0	0	30
12.5	38	44	153	0	0	0	22
13.5	24	55	95	0	0	0	19
14.5	26	69	71	0	0	0	2
15.5	20	94	33	0	0	0	0
16.5	5	86	2	0	0	0	1
17.5	1	85	0	0	0	0	0
18.5	1	66	0	0	0	0	0
19.5	0	47	0	0	0	0	0
S(cyc/time) :	415	715	746	0	56	0	380

Rainflow counts for file D_1997100713

Bins (in)	AS1 (cyc/time)	AS5 (cyc/time)	AS9 (cyc/time)	AS16 (cyc/time)	AS23 (cyc/time)	AS24 (cyc/time)	AN24 (cyc/time)
0.5	251	22	72	1051	59	561	72
1.5	59	24	27	167	172	416	47
2.5	30	25	46	1	248	24	25
3.5	28	17	60	0	267	0	36
4.5	20	27	43	0	94	0	33
5.5	42	53	50	0	3	0	64
6.5	30	52	15	0	0	0	56
7.5	37	93	27	0	0	0	113
8.5	59	66	42	0	0	0	146
9.5	57	91	42	0	0	0	128
10.5	38	89	27	0	0	0	87
11.5	53	120	59	0	0	0	26
12.5	21	106	100	0	0	0	6
13.5	29	80	61	0	0	0	5
14.5	23	60	79	0	0	0	0
15.5	28	22	40	0	0	0	0
16.5	12	1	33	0	0	0	0
17.5	9	0	24	0	0	0	0
18.5	2	0	37	0	0	0	0
19.5	0	0	4	0	0	0	0
S(cyc/time) :	828	948	888	1219	843	1001	844

Rainflow counts for file D_1997100713 excluding bins less than 3 in.

Bins (in)	AS1 (cyc/time)	AS5 (cyc/time)	AS9 (cyc/time)	AS16 (cyc/time)	AS23 (cyc/time)	AS24 (cyc/time)	AN24 (cyc/time)
0.5	0	0	0	0	0	0	0
1.5	0	0	0	0	0	0	0
2.5	0	0	0	0	0	0	0
3.5	28	17	60	0	267	0	36
4.5	20	27	43	0	94	0	33
5.5	42	53	50	0	3	0	64
6.5	30	52	15	0	0	0	56
7.5	37	93	27	0	0	0	113
8.5	59	66	42	0	0	0	146
9.5	57	91	42	0	0	0	128
10.5	38	89	27	0	0	0	87
11.5	53	120	59	0	0	0	26
12.5	21	106	100	0	0	0	6
13.5	29	80	61	0	0	0	5
14.5	23	60	79	0	0	0	0
15.5	28	22	40	0	0	0	0
16.5	12	1	33	0	0	0	0
17.5	9	0	24	0	0	0	0
18.5	2	0	37	0	0	0	0
19.5	0	0	4	0	0	0	0
S(cyc/time) :	488	877	743	0	364	0	700

Rainflow counts for file D_1997120718

Bins (in)	AS1 (cyc/time)	AS5 (cyc/time)	AS9 (cyc/time)	AS16 (cyc/time)	AS23 (cyc/time)	AS24 (cyc/time)	AN24 (cyc/time)
0.5	87	5	9	1250	527	538	211
1.5	0	0	1	203	248	418	27
2.5	0	4	0	2	144	71	33
3.5	1	7	0	0	65	6	103
4.5	16	18	0	0	42	0	85
5.5	44	27	0	0	12	0	91
6.5	90	42	0	0	1	0	53
7.5	102	72	15	0	0	0	77
8.5	113	59	29	0	0	0	93
9.5	74	77	55	0	0	0	54
10.5	49	57	70	0	0	0	30
11.5	26	55	61	0	0	0	29
12.5	29	69	110	0	0	0	22
13.5	10	80	87	0	0	0	10
14.5	3	63	65	0	0	0	20
15.5	0	64	73	0	0	0	7
16.5	0	81	88	0	0	0	1
17.5	0	51	54	0	0	0	0
18.5	0	48	34	0	0	0	0
19.5	0	72	6	0	0	0	0
S**(cyc/time) :**	644	951	757	1455	1039	1033	946

Rainflow counts for file D_1997120718 excluding bins less than 3 in.

Bins (in)	AS1 (cyc/time)	AS5 (cyc/time)	AS9 (cyc/time)	AS16 (cyc/time)	AS23 (cyc/time)	AS24 (cyc/time)	AN24 (cyc/time)
0.5	0	0	0	0	0	0	0
1.5	0	0	0	0	0	0	0
2.5	0	0	0	0	0	0	0
3.5	1	7	0	0	65	6	103
4.5	16	18	0	0	42	0	85
5.5	44	27	0	0	12	0	91
6.5	90	42	0	0	1	0	53
7.5	102	72	15	0	0	0	77
8.5	113	59	29	0	0	0	93
9.5	74	77	55	0	0	0	54
10.5	49	57	70	0	0	0	30
11.5	26	55	61	0	0	0	29
12.5	29	69	110	0	0	0	22
13.5	10	80	87	0	0	0	10
14.5	3	63	65	0	0	0	20
15.5	0	64	73	0	0	0	7
16.5	0	81	88	0	0	0	1
17.5	0	51	54	0	0	0	0
18.5	0	48	34	0	0	0	0
19.5	0	72	6	0	0	0	0
S**(cyc/time) :**	557	942	747	0	120	6	675

Rainflow counts for file D_1997120746

Bins (in)	AS1 (cyc/time)	AS5 (cyc/time)	AS9 (cyc/time)	AS16 (cyc/time)	AS23 (cyc/time)	AS24 (cyc/time)	AN24 (cyc/time)
0.5	486	34	40	839	810	110	255
1.5	74	5	0	218	292	111	14
2.5	54	0	0	17	104	119	28
3.5	67	3	0	0	26	161	18
4.5	49	8	0	0	2	199	42
5.5	17	9	0	0	1	137	45
6.5	8	11	2	0	0	13	39
7.5	4	9	23	0	0	1	42
8.5	18	17	61	0	0	0	61
9.5	36	31	55	0	0	0	62
10.5	81	24	78	0	0	0	51
11.5	39	32	60	0	0	0	36
12.5	10	34	72	0	0	0	31
13.5	5	19	73	0	0	0	24
14.5	0	25	51	0	0	0	11
15.5	0	14	64	0	0	0	2
16.5	0	12	77	0	0	0	2
17.5	0	10	83	0	0	0	0
18.5	0	14	38	0	0	0	0
19.5	0	442	10	0	0	0	0
S(cyc/time) :	948	753	787	1074	1235	851	763

Rainflow counts for file D_1997120746 excluding bins less than 3 in.

Bins (in)	AS1 (cyc/time)	AS5 (cyc/time)	AS9 (cyc/time)	AS16 (cyc/time)	AS23 (cyc/time)	AS24 (cyc/time)	AN24 (cyc/time)
0.5	0	0	0	0	0	0	0
1.5	0	0	0	0	0	0	0
2.5	0	0	0	0	0	0	0
3.5	67	3	0	0	26	161	18
4.5	49	8	0	0	2	199	42
5.5	17	9	0	0	1	137	45
6.5	8	11	2	0	0	13	39
7.5	4	9	23	0	0	1	42
8.5	18	17	61	0	0	0	61
9.5	36	31	55	0	0	0	62
10.5	81	24	78	0	0	0	51
11.5	39	32	60	0	0	0	36
12.5	10	34	72	0	0	0	31
13.5	5	19	73	0	0	0	24
14.5	0	25	51	0	0	0	11
15.5	0	14	64	0	0	0	2
16.5	0	12	77	0	0	0	2
17.5	0	10	83	0	0	0	0
18.5	0	14	38	0	0	0	0
19.5	0	442	10	0	0	0	0
S(cyc/time) :	334	714	747	0	29	511	466

Rainflow counts for file D_1998062816

Bins (in)	AS1 (cyc/time)	AS5 (cyc/time)	AS9 (cyc/time)	AS16 (cyc/time)	AS23 (cyc/time)	AS24 (cyc/time)	AN24 (cyc/time)
0.5	1278	788	209	62	28	32	434
1.5	6	0	0	6	18	3	324
2.5	0	0	0	0	25	0	174
3.5	0	0	0	0	28	0	45
4.5	0	0	0	0	37	0	2
5.5	0	0	0	0	26	0	0
6.5	0	0	0	0	20	0	0
7.5	0	0	0	34	42	0	0
8.5	0	0	0	59	36	1	0
9.5	0	0	0	50	24	7	0
10.5	0	0	0	19	24	0	0
11.5	0	0	0	22	54	9	0
12.5	0	0	0	25	52	14	0
13.5	0	0	0	48	55	18	0
14.5	0	0	0	64	40	13	0
15.5	0	0	0	108	50	18	0
16.5	0	0	0	74	49	37	0
17.5	0	0	0	79	25	70	0
18.5	0	0	0	89	60	112	0
19.5	0	0	0	80	150	272	0
S**(cyc/time) :**	1284	788	209	819	843	606	979

Rainflow counts for file D_1998062816 excluding bins less than 3 in.

Bins (in)	AS1 (cyc/time)	AS5 (cyc/time)	AS9 (cyc/time)	AS16 (cyc/time)	AS23 (cyc/time)	AS24 (cyc/time)	AN24 (cyc/time)
0.5	0	0	0	0	0	0	0
1.5	0	0	0	0	0	0	0
2.5	0	0	0	0	0	0	0
3.5	0	0	0	0	0	0	0
4.5	0	0	0	0	37	0	2
5.5	0	0	0	0	26	0	0
6.5	0	0	0	0	20	0	0
7.5	0	0	0	34	42	0	0
8.5	0	0	0	59	36	1	0
9.5	0	0	0	50	24	7	0
10.5	0	0	0	19	24	0	0
11.5	0	0	0	22	54	9	0
12.5	0	0	0	25	52	14	0
13.5	0	0	0	48	55	18	0
14.5	0	0	0	64	40	13	0
15.5	0	0	0	108	50	18	0
16.5	0	0	0	74	49	37	0
17.5	0	0	0	79	25	70	0
18.5	0	0	0	89	60	112	0
19.5	0	0	0	80	150	272	0
S**(cyc/time) :**	0	0	0	751	744	571	2

Rainflow counts for file D_1998062818

Bins (in)	AS1 (cyc/time)	AS5 (cyc/time)	AS9 (cyc/time)	AS16 (cyc/time)	AS23 (cyc/time)	AS24 (cyc/time)	AN24 (cyc/time)
0.5	1648	639	168	457	15	79	949
1.5	0	0	0	113	21	1	348
2.5	0	0	0	8	19	10	72
3.5	0	0	0	17	38	14	19
4.5	0	0	0	32	30	27	1
5.5	0	0	0	54	47	61	1
6.5	0	0	0	108	31	45	0
7.5	0	0	0	107	41	64	0
8.5	0	0	0	49	69	78	0
9.5	0	0	0	77	80	69	0
10.5	0	0	0	86	90	32	0
11.5	0	0	0	80	124	25	0
12.5	0	0	0	65	76	21	0
13.5	0	0	0	41	49	4	0
14.5	0	0	0	19	42	9	0
15.5	0	0	0	11	36	15	0
16.5	0	0	0	0	28	13	0
17.5	0	0	0	1	6	36	0
18.5	0	0	0	0	1	12	0
19.5	0	0	0	0	0	32	0
S**(cyc/time) :**	1648	639	168	1325	843	647	1390

Rainflow counts for file D_1998062818 excluding bins less than 3 in.

Bins (in)	AS1 (cyc/time)	AS5 (cyc/time)	AS9 (cyc/time)	AS16 (cyc/time)	AS23 (cyc/time)	AS24 (cyc/time)	AN24 (cyc/time)
0.5	0	0	0	0	0	0	0
1.5	0	0	0	0	0	0	0
2.5	0	0	0	0	0	0	0
3.5	0	0	0	0	0	0	0
4.5	0	0	0	32	30	27	1
5.5	0	0	0	54	47	61	1
6.5	0	0	0	108	31	45	0
7.5	0	0	0	107	41	64	0
8.5	0	0	0	49	69	78	0
9.5	0	0	0	77	80	69	0
10.5	0	0	0	86	90	32	0
11.5	0	0	0	80	124	25	0
12.5	0	0	0	65	76	21	0
13.5	0	0	0	41	49	4	0
14.5	0	0	0	19	42	9	0
15.5	0	0	0	11	36	15	0
16.5	0	0	0	0	28	13	0
17.5	0	0	0	1	6	36	0
18.5	0	0	0	0	1	12	0
19.5	0	0	0	0	0	32	0
S**(cyc/time) :**	0	0	0	730	750	543	2

References

ASTM E 1049-85 (1985), "Standard Practices for Cycle Counting in Fatigue Analysis," American Society for Testing and Materials, West Conshohocken, PA, Reapproved 1999.

Buhl M. (2002), "CRUNCH Users Manual," National Wind Technology Center at the National Renewable Energy Laboratory, Golden, Colorado

Downing, S. D. and Socie, D. F. (1982), "Simple Rainflow Counting Algorithms," International Journal of Fatigue, Vol. 4, No. 1, pp. 31-40.

Hudson, D. E. (1979), "Reading and Interpreting Strong Motion Accelerograms," Earthquake Engineering Research Institute, Engineering Monograph No. 1, Berkeley, CA.

Lamb, J. L. (1985), "Study of Simple Fatigue Resistant Anchorage for Cable-Stayed Applications", M.S. Thesis, Department of Civil Engineering, The University of Texas at Austin.

Main, J. A. (2000), "Characterization of Rain-Wind Induced Stay-Cable Vibrations from Full-Scale Measurements," NSF/STA Summer Institute Research Report, Saitama University, Saitama, Japan.

Main, J. A., Jones, N. P., and Yamaguchi, H., (2000), "Characterization of Rain-Wind Induced Stay-Cable Vibrations from Full-Scale Measurements", Johns Hopkins University, Baltimore, MD and Saitama University, Urawa, Saitama, Japan.

Papailiou, K. O. (1999), "On the Bending of Multi-Layer Strands," Wire, Vol. 49, No. 5, pp. 44-47.

Paulson, C., Frank, K., and Breen, J. (1983), "A Fatigue Study of Prestressing Strand," Research Report 300-1, Center for Transportation Research, Bureau of Engineering Research, The University of Texas at Austin, Austin, TX, April 1983.

Poser, Marcel (2001), "Full-Scale Bending Fatigue Tests on Stay Cables", M.S. Thesis, Department of Civil Engineering, The University of Texas at Austin.

Poston, R. W. and Kesner, Keith (1990), “Progress Report Number Two, Evaluation and Repair of Stay-Cable Vibrations, Fred Hartman Bridge, Veterans Memorial Bridge”, Whitlock Dalrymple Poston and Associates, Inc., Manassas, Virginia

PTI Guide Specification (2001), “Recommendations for Stay Cable Design, Testing and Installation”, Post-Tensioning Institute, Phoenix, AZ.

Sarker, P.P., Mehta, K.C., Zhao, Z., (1999), “Aerodynamic Approach to Control Vibrations in Stay-Cables,” Wind Engineering Research Center, Department of Civil Engineering, Texas Tech University, Lubbock, TX.

Timoshenko, S. (1956). "Strength of Materials: Part II - Advanced Theory and Problems," D.Van Nostrand Co., Inc., Princeton, NJ.